

# Effects of Overlapping Strings in $pp$ Collisions \*

---

**Christian Bierlich<sup>1</sup>, Gösta Gustafson<sup>1</sup>, Leif Lönnblad<sup>1</sup> and Andrey Tarasov<sup>2</sup>**

<sup>1</sup>*Dept. of Astronomy and Theoretical Physics, Lund University, Sweden*

<sup>2</sup>*Theory Group, Jefferson Lab, Newport News, Virginia, USA*

**ABSTRACT:** In models for hadron collisions based on string hadronization, the strings are usually treated as independent, allowing no interaction between the confined colour fields. In studies of nucleus collisions it has been suggested that strings close in space can fuse to form “colour ropes”. Such ropes are expected to give more strange particles and baryons, which also has been suggested as a signal for plasma formation. Overlapping strings can also be expected in  $pp$  collisions, where usually no phase transition is expected. In particular at the high LHC energies the expected density of strings is quite high. To investigate possible effects of rope formation, we present a model in which strings are allowed to combine into higher multiplets, giving rise to increased production of baryons and strangeness, or recombine into singlet structures and vanish. Also a crude model for strings recombining into junction structures is considered, again giving rise to increased baryon production. The models are implemented in the DIPSY MC event generator, using PYTHIA8 for hadronization, and comparison to  $pp$  minimum bias data, reveals improvement in the description of identified particle spectra.

**KEYWORDS:** Hadronization, QCD, Jets, Parton Model, Phenomenological Models, Colour Reconnection.

---

\*Work supported in part by the MCnetITN FP7 Marie Curie Initial Training Network, contract PITN-GA-2012-315877, the Swedish Research Council (contracts 621-2012-2283 and 621-2013-4287), and contract DE-AC05-06OR23177 under which the Jefferson Science Associates, LLC operate the Thomas Jefferson National Accelerator Facility.

---

## Contents

<b>1. Introduction</b>	<b>2</b>
<b>2. String fragmentation</b>	<b>4</b>
2.1 Tunneling	5
2.2 Space-time picture and longitudinal momentum distribution	6
2.3 Baryon production	7
2.4 Effects of a modified string tension	8
<b>3. Ropes</b>	<b>11</b>
3.1 Rope formation	11
3.2 Rope tension	11
3.3 Fragmentation of a rope	13
<b>4. Implementation of ropes in the DIPSY Generator</b>	<b>15</b>
4.1 The Final-state Swing	15
4.2 Estimates of overlap region	17
4.3 Exclusive observables with DIPSY	19
<b>5. Results</b>	<b>20</b>
5.1 Comparison to data	20
5.2 Model behaviour	22
5.3 Particle ratios and flow-like effects	25
<b>6. Conclusions and outlook</b>	<b>27</b>
<b>A. The DIPSY model</b>	<b>31</b>
A.1 The initial-state Swing mechanism	32
<b>B. Colour algebra</b>	<b>33</b>
B.1 Calculation of $p$ and $q$	33
B.2 An illustrative example	34
<b>C. Detailed description of the rope models</b>	<b>35</b>
C.1 A pipe-based treatment	36
C.2 A dipole-based treatment	38
C.3 Implementation details	39
<b>D. Tuning</b>	<b>40</b>
D.1 Tuning final-state shower and hadronization	40
D.2 Tuning DIPSY	41

## 1. Introduction

In most models for high energy collisions, like the popular PYTHIA [1] or HERWIG [2] models, the hadronization mechanism is described via strings or cluster chains. The strings are often treated as independent, but in connection with nucleus collisions it was early suggested that the many strings produced within a limited space may interact and form "colour ropes" [3,4]. Such ropes have subsequently been studied by many authors with applications to high energy nucleus collisions [5–11]. The stronger field in a rope is expected to give larger rates for strangeness and baryons. The effect on the multiplicity is more difficult to predict, and here the results depend on simplified assumptions, often without a real motivation. Usually the result is either a decreased or an unmodified particle multiplicity.

As rope formation is expected to give increased rates of strange particles and baryons, which may mimic effects of plasma formation, it makes signals for a phase transition more difficult to interpret. It has also been suggested that ropes may initiate the formation of a quark–gluon plasma [6, 12–14]. At LHC energies many overlapping strings are also expected in  $pp$  scattering, where plasma formation normally is not expected. In this paper we want to study string interference effects in  $pp$  scattering, with the aim to get a better understanding of the dynamics in  $pp$  collisions, and simultaneously get a tool to estimate possible rope effects in nucleus collisions.

For a quantitative estimate of interaction between neighbouring strings, we believe it is essential to have a description formulated in transverse coordinate space. Such a formulation is also suitable for including effects of saturation for small  $x$  and high gluon densities. Here we will use the Lund dipole cascade model implemented in the event generator DIPSY [15, 16]. This model is based on a formulation of BFKL dynamics in transverse coordinate space, including non-leading-log and saturation effects, and also taking fluctuations and correlations into account.<sup>1</sup>

The Lund string hadronization model [22, 23]<sup>2</sup>, which has been particularly successful in describing data from  $e^+e^-$  annihilation at LEP [26, 27], is based on the assumption that a confined colour field between a quark and an antiquark is compressed to a linear flux tube, similar to a vortex line in a superconductor. When the string is stretched between separated colour charges, it can break by the production of  $q\bar{q}$  pairs [28–31] in a process similar to the production of  $e^+e^-$  pairs in a homogeneous electric field [32]. As demonstrated in ref. [33], this can be interpreted as the effect of a quantum-mechanical tunneling process. In the Lund model the dynamical motion of the flux tube is approximated by an infinitely thin *massless relativistic string*, and gluons are identified with transverse excitations on such a string [23], which also has the effect that the model is infrared stable, *i.e.* insensitive to soft or collinear gluons.

It was early observed that when the string hadronization model is tuned to LEP data,

---

<sup>1</sup>String interaction effects in  $pp$  collisions have also earlier been included in the event generator DTU-JET [17], formulated in momentum space. This was generalized to nucleus collisions, including a geometric distribution of nucleons within a nucleus [18]. Rope effects are also included, together with hadron rescattering, in the RQMD model, with applications in the SPS fixed target and RHIC energy ranges [19–21].

<sup>2</sup>For a review of the Lund hadronization model see ref. [24], or a more recent summary in ref. [25].

it slightly underestimates the production of strange particles in hadronic collisions [34]. Similarly in DIS, the LEP tune works well in the current fragmentation region (in the Breit frame), while in the proton fragmentation end, one again observes an enhanced strange quark fraction [35]. This effect is enhanced in data from LHC, where a rather dramatic increase is observed in the fractions of strange particles and baryons, most notably that of strange baryons [36]. These observations should not be surprising. The colour flux tubes are expected to have a transverse width determined by the confinement scale, of  $\sim 1$  fm. In  $pp$  collisions there can be several strings close to each other, and it should actually be rather surprising that models neglecting mutual string interaction are working as well as they do.

Biro *et al.* noted in ref. [3], that the colour charge at the endpoint of a rope formed by strings with random colour charges, is given by a random walk in colour space. The rope can break up in a stepwise manner by repeated production of  $q\bar{q}$  pairs, as expected from a local interaction  $\propto j_\mu A_\mu \sim \bar{\psi}\gamma_\mu\psi A_\mu$ . This process is analogous to the production of  $e^+e^-$  pairs in an electric field. It was pointed out in ref. [3] that for a rope formed by random charges, the number of pairs produced before a total breakup of the rope is in general smaller than the number of initial strings, and also that the total time for this successive split is approximately the same as for a single string.

Although such a stepwise breakup of a rope is assumed in most studies, also an immediate breakup by production of multi-quark–antiquark systems has been advocated by Amelin, Braun, and Pajares [10] (also mentioned as a possibility in ref. [3]), and a breakup by the production of gluon pairs has been studied by Gyulassy and Iwazaki [6]. It has also been suggested that a rapid decay of the ropes into elementary partons is facilitating the formation of a quark–gluon plasma [6, 13, 14].

It was early suggested that, if the charges correspond to a specific SU(3) multiplet, the tension (or energy density) in the rope is given by the second Casimir operator [37]. For an isolated rope this conjecture has later been supported by lattice calculations [38]. However, if the rope is surrounded by other strings or ropes, we expect that the transverse area, and thus the rope tension, will be affected by the presence of the neighbouring ropes, which exert a pressure keeping the radius small. Such a pressure might also cause a collective expansion contributing to extra transverse momentum for the hadrons. It ought to be kept in mind, that this feature contributes to the necessary uncertainties in estimating the effects of rope formation.

As mentioned above we will here use the event generator DIPSY to study the effects of string interaction and rope formation in more detail, beyond qualitative results such as increased strangeness and baryon production. The DIPSY model is a generalization and extension of Mueller’s dipole model [39–41], which describes BFKL evolution in transverse coordinate space. At high energies the high density of soft gluons effectively screens colour charges, thus suppressing gluons with  $p_\perp$  below a saturation scale  $Q_s$ . As in the Color Glass Condensate formalism for nucleus collisions [42, 43], we argue that this is a motivation for a perturbative treatment of the initial phase in terms of quarks and gluons. (This is also assumed in other models for soft interactions, like PYTHIA and HERWIG.)

While Mueller’s model reproduces leading log BFKL evolution, the DIPSY model in-

cludes essential non-leading corrections to BFKL, as well as saturation within the cascade evolution, and confinement. It reproduces total, elastic, and diffractive cross sections in  $pp$  collisions and DIS, and gives a good description of particle distributions in minimum-bias final states [16]. However, as parton distributions are generated within the model, and therefore not tuned to data, and are in addition limited to gluons, the model is naturally less accurate than *e.g.* the PYTHIA and HERWIG models. Our aim has instead been focused on understanding the dynamics of small- $x$  evolution and saturation, including correlations and fluctuations, *e.g.* in connection with multiple parton interactions [44] and diffraction [45,46]. The formulation in transverse coordinate space makes the DIPSY model particularly suited for studies of string interference and rope formation. Although it has also been applied to collisions with nuclei (see *e.g.* refs. [47,48]), we will in this paper limit our study to proton–proton collisions.

We will here assume that colour ropes can form by coherent interaction between a group of strings confined within a limited transverse size. As in ref. [3] we assume random colour charges for the individual strings, leading to a random walk in colour space. We also assume that the rope breaks by successive production of new  $q\bar{q}$  pairs. The nature of the tunneling process implies here that an “effective string tension” is determined by the *reduction* in rope tension in each individual breakup. As mentioned in ref. [3], and discussed in detail below, the result of the rope formation is then a smaller number of  $q\bar{q}$  pairs needed to break the rope, but a larger effective string tension. As is generally expected, this implies larger strangeness and baryon fractions. In addition our model also gives nontrivial effects on the  $p_{\perp}$ -dependence for different particle ratios, which to some extent mimic effects of transverse flow. In this paper we present results where the model (with some approximations) is compared to LHC  $pp$  scattering data, with encouraging qualitative agreement. In the future we plan to also study effects of rope formation in collisions with nuclei. We begin this article with a recapitulation of the relevant ingredients of the Lund string fragmentation in section 2, before we describe the basic idea of the rope model in section 3. Then we describe the proposed “final-state swing mechanism” together with the implementation of our rope model in the interface between DIPSY and PYTHIA8 in section 4. In section 5 we present some first results, and finally in section 6 we summarize our findings and give an outlook.

For completeness, we end the article with a number of appendices. There we first summarize details in the DIPSY model (appendix A) that are important for our rope implementation, and also summarize the relevant colour algebra needed (appendix B). Most of this can be found in various different references, but we think it is valuable to have the relevant issues collected here. Furthermore, we have collected some of the more technical points in our implementation and in the tuning procedure in appendices C and D respectively. Although these are important for our results, they tend to hamper the readability of the main text, and are therefore presented separately.

## 2. String fragmentation

In this section we will discuss the fragmentation of a single string. We first discuss the

basic tunneling process, then the space-time picture describing how the produced quarks and antiquarks combine to hadrons, followed by a discussion of baryon production and spin effects. We end by a discussion of the effects of a modified effective string tension.

## 2.1 Tunneling

A linear colour electric field stretched between a quark and an antiquark, moving in opposite directions, can break up by the production of new  $q\bar{q}$  pairs, in a way similar to the production of  $e^+e^-$  pairs in a homogenous electric field. As discussed by Schwinger [32] the electric field is unstable, and the decay can be interpreted as the result of the production of new  $e^+e^-$  pairs with a rate per unit time and unit volume given by:

$$\mathcal{P} \propto (e\mathcal{E})^2 \exp\left(-\frac{\pi\mu^2}{e\mathcal{E}}\right). \quad (2.1)$$

Here  $\mu$  is the electron mass and  $\mathcal{E}$  the electric field strength. Thus  $e\mathcal{E}$  is the force acting on the produced electron or positron. As pointed out in ref. [33], this result can be interpreted as the effect of a tunneling process. Classically the electron and the positron cannot be produced in a point, but only separated by a distance  $2\mu/e\mathcal{E}$ , such that the reduction in the electric field energy can be transferred into the mass of the pair. In quantum theory the particles are produced locally by an interaction Lagrangian  $\sim e\bar{\psi}(x)\gamma_\mu\psi(x)A_\mu(x)$ , and have to tunnel through the classically forbidden region, where the wavefunctions can be estimated by the WKB method.

When generalizing this result to  $q\bar{q}$  pair production [28–31] in a linear confined colour field, the tunneling mechanism implies that  $e\mathcal{E}$  has to be replaced by the force acting on a quark, *i.e.* by the string tension<sup>3</sup>  $\kappa \sim 1$  GeV/fm. For the production of a pair with opposite transverse momenta  $p_\perp$  in this process, the mass  $\mu$  in eq. (2.1) will be replaced by the transverse mass  $\sqrt{\mu^2 + p_\perp^2}$ . This gives

$$\frac{d\mathcal{P}}{d^2p_\perp} \propto \kappa \exp\left(-\frac{\pi}{\kappa}(\mu^2 + p_\perp^2)\right), \quad (2.2)$$

which integrated over  $p_\perp$  gives the result in eq. (2.1), with the replacement  $e\mathcal{E} \rightarrow \kappa$ .

The result in eq. (2.2) can be used to estimate the relative production of quarks with different flavour, and the distribution in  $p_\perp$ . As it is not possible to theoretically determine the effective quark masses to be used in eq. (2.2), it is in practice necessary to tune the  $s/u$  ratio to experimental data. Fits to LEP data give  $s/u \approx 0.2$  [26, 27], which is not inconsistent with eq. (2.2) for reasonable quark masses. This mechanism also implies that

---

<sup>3</sup>In ref. [28]  $e\mathcal{E}$  was (for a quark with charge  $g/2$ ) replaced by  $g\mathcal{E}/2 = 2\kappa$ , where the string tension  $\kappa$  was estimated from the energy in the colour-electric field. However, ref. [31] noted that, although the force on the electron is given by  $e\mathcal{E}$  in a classical (macroscopic) electric field, in case the flux corresponds to only a single charge quantum, an extra contribution comes from the decreased field between the created quark and antiquark, giving  $e\mathcal{E} \mapsto g\mathcal{E}/4$ , just corresponding to the energy in the colour-electric field. In ref. [31] it was also noted that if the flux tube is embedded in a vacuum condensate, a further contribution to the string tension is given by the response from the condensate. In the bag model (similar to a type I superconductor) this contribution equals the energy in the colour-electric field.

charm and heavier quarks cannot be produced in the soft hadronization process; they can only be produced in an initial perturbative phase. For the transverse momenta it gives a Gaussian  $p_{\perp}$ -distribution with  $\sqrt{\langle p_{\perp}^2 \rangle} \approx 0.25$  GeV. Phenomenological fits to data will, however, also include effects from soft gluons below a necessary  $p_{\perp}$  cut in the perturbative parton shower. Tunes to data therefore give a somewhat wider distribution, with a width  $\sigma_{p_{\perp}} \approx 0.32$  GeV.

## 2.2 Space-time picture and longitudinal momentum distribution

The strange quark fraction and the  $p_{\perp}$ -distribution are governed by the tunneling mechanism, but for the longitudinal momentum distribution it is essential to take into account how the produced quarks and antiquarks can fit into a mesonic wavefunction, and combine to form final-state hadrons. The Lund fragmentation model is here inspired by the area law for Wilson loop integrals for a confining theory [49], in analogy with the Nambu-Goto action for a massless relativistic string. The boost invariance of the relativistic string (and of a linear homogenous electric field) has to result in a boost-invariant distribution of hadrons, produced around a hyperbola in space-time.

Consider, for simplicity, a model in one space dimension with only one quark flavour and a single mesonic state with mass  $m$ . In the Lund hadronization model the probability,  $\mathcal{P}$ , for the production of a specific state with  $n$  mesons with momenta  $p_i$  ( $i = 1, \dots, n$ ) is given by the relation [22]:

$$\mathcal{P} \propto \left\{ \left[ \prod_1^n N d^2 p_i \delta(p_i^2 - m^2) \right] \delta^{(2)}(\sum p_i - P_{tot}) \right\} \exp(-bA). \quad (2.3)$$

Here the term in curly parenthesis is a phase space factor, where the dimensionless constant  $N$  determines the relative weight between states with different number of mesons. The term  $bA$  in the exponent corresponds to the imaginary part of the action for the massless string, which is responsible for the decay and finite lifetime of the string.  $A$  is a measure of the space-time area covered by the string before the breakup, and  $b$  is a constant. Conventionally the area  $A$  is scaled by the square of the string tension  $\kappa$ :

$$A \equiv \mathcal{A} \kappa^2, \quad (2.4)$$

where  $\mathcal{A}$  is the area in space and time. Consequently the dimension of  $b$  is  $(energy)^{-2}$ .

The result in eq. (2.3) can be generated in a Monte Carlo simulation by producing the mesons in an iterative way starting from one of the string ends, where each meson takes a fraction  $z$  of the remaining energy. In each step the relevant  $z$ -value is given by the probability distribution or splitting function:

$$f(z) = N \frac{(1-z)^a}{z} e^{-bm^2/z}. \quad (2.5)$$

Here the constant  $a$  is related to  $N$  and  $b$  through the normalization constraint  $\int f(z) dz = 1$ . The production points for the pairs will be located around a hyperbola in space-time, with a typical proper time determined by

$$\langle \tau^2 \rangle = \frac{1+a}{b \kappa^2}. \quad (2.6)$$

This timescale is also related to the particle multiplicity via the relation

$$dN/dy \sim \sqrt{\langle \tau^2 \rangle} \kappa/m = \sqrt{\frac{1+a}{bm^2}}. \quad (2.7)$$

We note that absorbing the string tension in the definition of  $b$ , via the scaling in eq. (2.4), implies that  $\kappa$  does not appear explicitly in this expression for the splitting function or the particle density.

In three dimensions the hadron mass  $m$  in eqs. (2.3), (2.5), and (2.7) has to be replaced by the transverse mass  $m_{\perp} = \sqrt{m^2 + p_{\perp}^2}$ , in accordance with eq. (2.2). The parameters  $a$  and  $b$ , determined by the hadronic phase space and (the imaginary part of) the string action, have been tuned to LEP data, which in our case gives  $a = 0.42$  and  $b = 0.4$ .

### 2.3 Baryon production

Besides including different quark species, the relations in eqs. (2.3) and (2.5) must also be generalized to include baryon production and effects of spin interaction. A quark and an antiquark can combine to a total spin 1 or 0. Fits to data favour a  $\pi : \rho$  ratio about 1 : 1 (rather than the 1 : 3 expected from naive spin counting), which also can be understood as a result of normalization of the wavefunction in the tunneling process [24, 50].

A baryon–antibaryon pair can be formed if the string can break by the production of a diquark–antidiquark pair forming an antitriplet and a triplet respectively [51]. Such a process would be suppressed by a larger effective diquark mass. In this case the  $\bar{B}B$  pair will always have two quark flavours in common, in conflict with experimental data from  $e^+e^-$  annihilation. A modified model with a stepwise production mechanism (called the popcorn model) was presented in [52], and has since been incorporated in PYTHIA.<sup>4</sup> In a red–antired ( $r\bar{r}$ ) string-field a  $g\bar{g}$  quark pair can be produced as a vacuum fluctuation (see figures 1a and 1b). If the  $r$  and  $g$  charges form a  $\bar{b}$  antitriplet, a  $\bar{b}b$  field can be formed between the new quarks, which means that the net force on the green quark or antiquark is zero. During this fluctuation a  $b\bar{b}$  pair produced in the string can split the system by an effective diquark–anti-diquark production (see figure 1c). In this way one (or more) mesons can be produced between the baryon and antibaryon.

As hadronization is a non-perturbative process, estimating all possible hadron species in an MC implementation necessarily implies a set of additional phenomenological parameters, which all have to be tuned to experimental data. Although PYTHIA has adopted the popcorn model, it is reformulated in terms of diquark breakups with an additional probability for having mesons produced in between baryon pairs as in figure 1d. Most important for the result is therefore the diquark/quark ratio in the splitting process, together with the extra suppression of strange diquarks beyond the  $s/u$  suppression. A detailed description of the parameters involved in baryon production within the Lund model is presented in appendix C.

We here also want to point out that, besides the different parameters, it is also very important to take into account that a produced baryon must be symmetric in flavour and spin, in order to preserve SU(3) flavour symmetry (as is done in the PYTHIA generator).

---

<sup>4</sup>A stepwise production mechanism was suggested by Casher *et al.* in ref. [28].



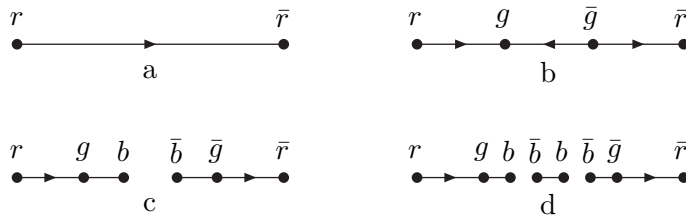


**Figure 1:** Illustration of popcorn production of a diquark pair. In frame a) no fluctuation has occurred, and a full string is spanned between a red–antired  $q\bar{q}$  pair. In frame b) a green–antigreen pair has appeared on the string as a quantum fluctuation. If the red and green quarks form an antiblue triplet, this reverses the colour flow in this part of the string, and the net force acting on the green quark is zero. In frame c) the string breaks by the production of a  $b\bar{b}$  pair, resulting in two string pieces with diquark ends. In frame d) another breakup in the blue triplet field results in an additional meson.

## 2.4 Effects of a modified string tension

We will in this paper assume that a rope breaks up by the repeated production of  $q\bar{q}$  pairs, as expected from an analogy with  $e^+e^-$  pair production in QED. As mentioned in the introduction, and discussed in detail in section 3, a rope formed by  $n$  elementary strings with random charges, can in general be fully extinguished by a number of  $q\bar{q}$  pairs smaller than or equal to  $n$ . Here  $n$  breakups will be needed in case the colour charges combine to the highest possible multiplet. As can be understood from the tunneling mechanism, the ”effective string tension”, to be inserted in eqs. (2.1) and (2.2) for each step, is determined by the energy released in the step. This means the *reduction* in rope tension when the new  $q\bar{q}$  pair is produced. We will therefore treat one step in the breakup of the rope, as the breakup of an individual string, with a modified effective string tension.

### 2.4.1 Effects on particle ratios

As discussed above, strangeness and baryon production is in the PYTHIA implementation determined by a set of phenomenological parameters, some of which represent the relative tunneling probabilities for different quarks and diquarks. Let the modification of the string tension be given by a simple scaling with an enhancement factor  $h$ , such that  $\kappa \mapsto \tilde{\kappa} = h\kappa$ . The result in eq. (2.1) or (2.2) then implies that the  $s/u$  ratio (called  $\rho$ ), will be modified by the scaling relation

$$\rho \mapsto \tilde{\rho} = \rho^{1/h}. \quad (2.8)$$

Baryon production in the popcorn model is somewhat more complicated. Here we will assume that the production of the vacuum fluctuation giving the first new pair in figure 1b is insensitive to the string tension<sup>5</sup>, while the production of the second pair shown in figure 1c, where the string breaks, is the result of a tunneling process. This means that we expect the same kind of scaling as for the  $s/u$  ratio in eq. (2.8) for the parameters

<sup>5</sup>Also if the fluctuation probability does depend on the string tension, it turns out that this effect can be compensated by a change in the effective coherence radius for the rope formation, described in section 4.2.

which determine the extra suppression of diquarks with strange quark content relative to diquarks without strange quarks, and the suppression of spin 1 diquarks relative to spin 0 diquarks. As these parameters go together with others that are not affected by string overlapping in defining the final diquark/quark ratio (called  $\xi$ ), the resulting expression for the mapping becomes

$$\xi \mapsto \tilde{\xi} = \tilde{\alpha}\beta \left( \frac{\xi}{\alpha\beta} \right)^{1/h}. \quad (2.9)$$

The parameter  $\alpha$  contains the parameters for all different types of diquark content, as mentioned above, and thus maps accordingly. The  $\beta$ -parameter is the popcorn fluctuation probability which in this work is assumed to be unaffected by changes in string tension. The complete mapping relation is derived in full in appendix C.

The effect of a modified string tension on the  $s/u$  ratio and the net diquark/quark ratio is presented in figure 2. The range of  $h$  chosen in figure 2 is much larger than the range relevant for the  $pp$  collisions considered in this work (which generally have  $h < 1.5$ ), but is chosen to show effects for large values of  $h$  relevant for heavy ion collisions<sup>6</sup>.

The tunneling probability in eq. (2.2) will also give somewhat increased transverse momenta, but as the tunneling effect is a minor contribution to the  $p_{\perp}$ -distribution, this effect is rather small. A detailed description of the above modifications is presented in appendix C.

#### 2.4.2 Effects on multiplicity

One could assume, that the factor  $\kappa^2$  in the production rate in eq. (2.1) should imply a change in the  $b$ -parameter in eqs. (2.3) and (2.5), and thus significantly modify hadron multiplicities. The quantity  $\mathcal{P}$  in eq. (2.1) is the probability per unit volume and unit time. In a one-dimensional string, it should be interpreted as probability per unit length and unit time. Therefore the space-time distance between break-up points is expected to be proportional to  $1/\kappa$ . At the same time the “yo-yo” states representing mesons have extension and oscillation times proportional to  $1/\kappa$ . Thus the earlier production time is compensated by the smaller string length needed to form a meson. This is taken into account via the scaling factor  $\kappa^2$  in eq. (2.4), with the effect that  $b$  is essentially unchanged. (For  $u$  and  $d$  quarks, with masses of the order 10 MeV, and a single string with tension  $\kappa \approx 0.2 \text{ GeV}^2$ , the exponential factor in eq. (2.1) is very close to 1, and therefore not significantly changed by an increased string tension.) The second free parameter in the model (when flavours and spin are neglected) is the parameter  $N$  in eq. (2.3), which specifies the relative weights between hadron states with different multiplicities. As the density of hadronic states ought to be independent of the former colour configuration, we do not expect any change in the  $N$ -parameter, although we admit that such modifications cannot be excluded when the mesons are produced in a stronger field.

Although the  $b$ -parameter would be unchanged if only light quarks were produced, it will increase slightly due to the enhanced production probability for strange quarks and

---

<sup>6</sup>We note that the PYTHIA implementation currently limits all suppression parameters from above at a value of one, corresponding to the situation where the suppression is gone. The parameter  $\tilde{\xi}$  can in principle take on larger values and will, with  $\beta = 0.25$ , saturate at  $\tilde{\xi} = 1.75$ .

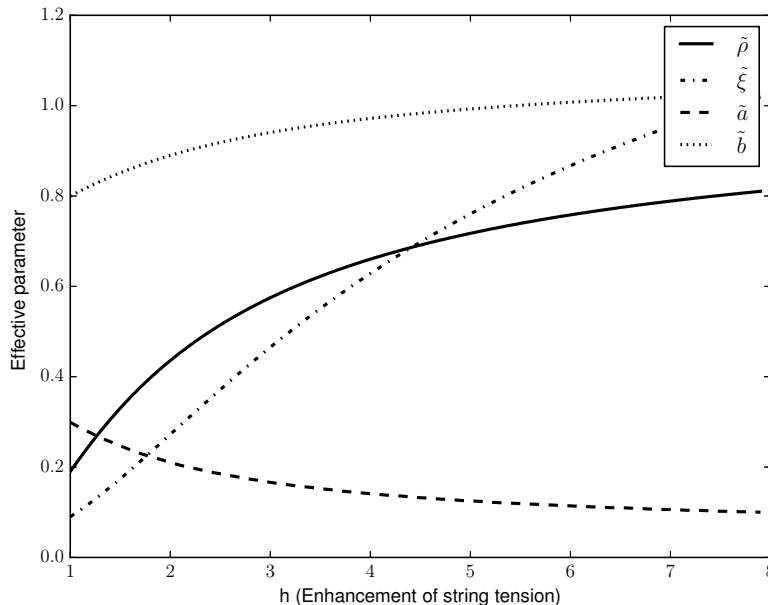


**Figure 2:** Effective parameters of the string model as a function of effective string tension. The parameters  $\rho$  and  $\xi$  control the strangeness content and baryonic content respectively,  $a$  and  $b$  are related to multiplicity. A modified string tension has a sizeable effect on  $\rho$  and  $\xi$  in particular. The range of  $h$  shown is much larger than relevant for  $pp$  collisions, which typically have  $h < 1.5$ . Larger values of  $h$  are, however, relevant for heavy ion collisions. The values of the parameters for  $h = 1$  comes from a tune to LEP data.

diquarks, given by an increased exponential factor in eq. (2.1). This gives a shift

$$b \mapsto \tilde{b} = \frac{2 + \tilde{\rho}}{2 + \rho} b. \quad (2.10)$$

As the  $a$ -parameter is calculated from the normalization constraint for the splitting function in eq. (2.5), it will get a correspondingly moderate modification. The effect on the parameters  $a$  and  $b$  is also shown in figure 2, and we see that these parameters are less affected by an increased string tension than the parameters determining strangeness and baryon ratios. As it will be discussed in section 5.2, a typical value for the string tension enhancement factor  $h$  at LHC is around 1.2. Changes in  $a$  and  $b$  could therefore naively account for  $\sim 5\%$  decrease in multiplicity in  $pp$ , as particle density is approximately proportional to  $\sqrt{(1+a)/b}$  (see eq. (2.7)). Since some parameters must be retuned after implementation of the rope model, this effect will not appear in final state observables (note that the string hadronization parameters are still tuned to LEP data, see appendix D for a detailed account of the tuning procedure.) The model should, however, not be further retuned when it is applied to nucleus collisions at LHC energies. Here  $h$  is expected to be so large, that a decrease of the order 15 – 20% in multiplicity, due to changes in  $\tilde{a}$  and  $\tilde{b}$ , is a prediction of the model.

### 3. Ropes

In this section an ideal situation is considered, where separated colour charges within a limited area in transverse space act coherently to form a colour rope (assuming that the total system is a colour singlet.) As mentioned in the introduction, lattice calculations show that if the endpoint charges correspond to a specific SU(3) multiplet, the tension (or energy density) in the rope is given by the second Casimir operator [38]. This result is valid for an isolated rope, modifications must be expected in a situation where the rope is surrounded by other ropes or strings. Here we discuss the formation of a rope, its tension, and its eventual decay.

#### 3.1 Rope formation

We study a situation, where a rope is formed by a group of ordinary triplet–antitriplet strings, where the net colour charge is obtained from the addition of  $m$  colour triplets and  $n$  antitriplets with random colours. As pointed out first in ref. [3], the result corresponds to a kind of random walk in colour space. A detailed discussion of this process can be found *e.g.* in ref. [53] or in appendix B.1. Here we only present the main features essential for the later discussion.

While in SU(2) a multiplet is specified by the quantum number  $j$ , or its multiplicity  $(2j + 1)$ , an SU(3) multiplet can be specified by two quantum numbers  $p$  and  $q$ . A specific state then corresponds to  $p$  coherent triplets (*e.g.* all red) and  $q$  coherent antitriplets (*e.g.* all antigreen). In addition the triplet and the antitriplet must be in an octet state (as is the case for red–antigreen), and not a singlet. The multiplicity,  $N$ , of the multiplet  $\{p, q\}$  is then given by:

$$N = \frac{1}{2}(p + 1)(q + 1)(p + q + 2). \quad (3.1)$$

The result of adding a set of triplets and antitriplets can be calculated in an iterative way. Starting from a multiplet  $\{p, q\}$  adding one more triplet, with random colour, one obtains the multiplets

$$\{p + 1, q\}, \quad \{p - 1, q + 1\}, \quad \text{and} \quad \{p, q - 1\}, \quad (3.2)$$

with weights proportional to the corresponding multiplicities given by eq. (3.1). From symmetry, the addition of an antitriplet gives the multiplets  $\{p, q + 1\}$ ,  $\{p + 1, q - 1\}$ , and  $\{p - 1, q\}$ . Multiplets with negative values for  $p$  or  $q$  are not allowed. In appendix B.1 the result for adding random colour octets (corresponding to gluons) is also described.

The average walk can be easily calculated numerically, and in figure 3 we show  $\langle p + q \rangle$  obtained from randomly adding triplets and antitriplets, with a fixed number,  $m + n$ , of charges. (The individual numbers  $m$  and  $n$  are then given by a binomial distribution. The same result was also presented in ref. [3].) The width of the distribution is indicated by the band showing  $1\sigma$  variations.

#### 3.2 Rope tension

As mentioned in the introduction, lattice calculations show that the tension in an isolated static rope is proportional to the quadratic Casimir operator  $C_2$  [38]. The Casimir operator

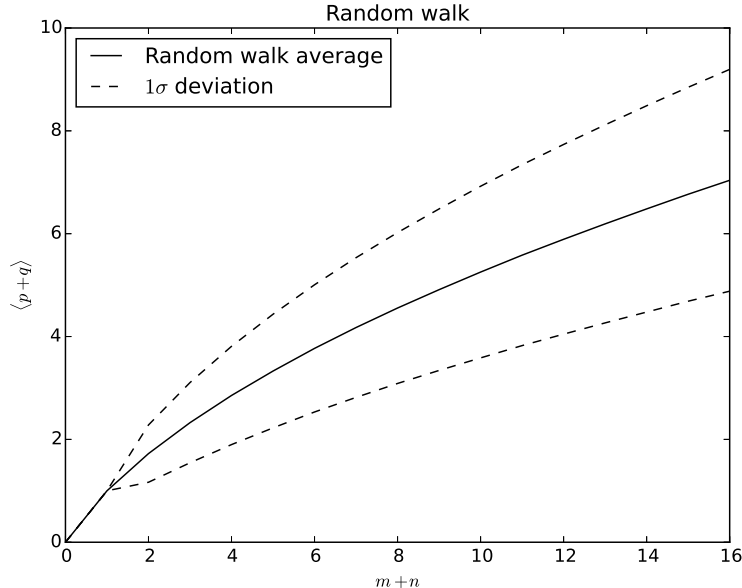


**Figure 3:** Relation between  $\langle p + q \rangle$  and  $m + n$  after a random walk in  $p, q$ -space. The shaded area corresponds to the standard deviation around the average  $\langle p + q \rangle$ .

is only defined up to a normalization constant, but for our purpose we only need the value of  $C_2$  normalized to a triplet (antitriplet)  $\{1, 0\}$  ( $\{0, 1\}$ ), corresponding to the tension in a single string. This is given by

$$C_2(\{p, q\})/C_2(\{1, 0\}) = \frac{1}{4} (p^2 + pq + q^2 + 3p + 3q), \quad (3.3)$$

which thus can be regarded as the relative strength of the “rope tension”.

It is, however, possible that the energy is increased if the transverse area is constrained by neighbouring ropes and strings. This effect is very hard to estimate, and contributes to the uncertainties in the predictions from string interactions. To illustrate this problem we first look at the analogous situation in a normal superconductor. Here a longitudinal magnetic flux is confined by currents in the surrounding condensate. In an extreme type I superconductor the surface energy is small, and a tube with two flux quanta will have doubled cross section and doubled energy. If, however, the flux tube would be constrained within the same transverse area, the magnetic field energy will be multiplied by 4, but the energy to annihilate the condensate within the tube (originally equal to the field energy) will be unchanged. The net result is a change by a factor 2.5. In a type II superconductor the magnetic flux and the energy density are more concentrated close to the center of a flux tube or vortex line, and there is a repulsive (attractive) interaction between parallel (antiparallel) vortices, with a logarithmic dependence on the separation.

The simplest model for a colour flux tube is the bag model [54,55], which is analogous to a type I superconductor. The tension in an unconstrained flux tube is here proportional to  $\sqrt{C_2}$  [55], in contradiction to the lattice result. However, for a flux tube constrained to

the width of an elementary string, the energy is indeed proportional to the lattice result  $C_2$  [56].

Lattice calculations by Cardoso *et al.* [57] show that the energy in the longitudinal colour-electric field is dominating over the transverse colour-magnetic field, with other components small, and the result shows similarities with a type II superconductor. However, recent calculations by Cea *et al.* [58] indicate, that the best analogy with a dual superconductor is close to the transition between type I and type II, but with the Ginzburg–Landau parameter within the type I region.

We conclude that there are considerable uncertainties in the estimation of the tension in a rope. Fortunately it turns out that, for the results presented here, the effects of a modified effective rope tension can be compensated by a modified value for the effective rope width  $r_0$ . We will therefore in the following assume that the tension is proportional to the Casimir operator of the colour multiplet, in accordance with the lattice calculations for an isolated rope.

### 3.3 Fragmentation of a rope

#### 3.3.1 Effective string tension and particle ratios

As in most studies of rope fragmentation, we will assume that the colour rope will break up in a stepwise manner, by the production of quark–antiquark pairs. This is the result for an interaction Lagrangian proportional to  $\bar{\psi}\gamma_\mu\psi A_\mu$ . In the region between the newly produced quark and antiquark, the field corresponding to the  $\{p, q\}$  multiplet can be reduced to either a  $\{p-1, q\}$  or a  $\{p, q-1\}$  multiplet. In the first case the antiquark is pulled towards the  $\{p, q\}$  charge (and the quark towards the  $\{q, p\}$  charge in the other end of the rope), and in the second case it is pulled in the opposite direction. As discussed in section 2.4, an essential point is that the energy released in the breakup is what enters in the tunneling process discussed in section 2.1, and thus determines the production probabilities in eqs. (2.1) and (2.2). This is given by the *difference* between the Casimir operators for the multiplets  $\{p, q\}$  and  $\{p-1, q\}$  or  $\{p, q-1\}$  respectively. This difference thus represents an *effective string tension*, or  $\tilde{\kappa}$ , introduced in section 2.4.

For a breakup via the transition  $\{p, q\} \rightarrow \{p-1, q\}$  we get from eq. (3.3) the effective string tension

$$\tilde{\kappa} = \frac{2p+q+2}{4}\kappa. \quad (3.4)$$

We note that for large charges  $p$  this result grows  $\sim (p/2)\kappa$ , (*i.e.* more slowly than  $\propto p\kappa$ ). As an example we have for a rope consisting of two parallel strings in a  $\{2,0\}$ -state the Casimir operator  $C_2(\{2,0\}) = 5/2 \times C_2(\{1,0\})$ . In the first breakup the effective string tension will then be  $\tilde{\kappa} = (5/2 - 1)\kappa = (3/2)\kappa$ , while for the second break-up we will have the normal tension  $\tilde{\kappa} = \kappa$ . A more complicated example is presented in appendix B.2.

We want to emphasize that this result is significantly smaller than what is assumed in most studies of rope effects. Although the change in rope tension is used *e.g.* in ref. [7], it is quite common to use Schwinger’s result in eq. (2.1), with a constant field  $\mathcal{E}$  proportional to the charge  $Q$ . This would correspond to a situation where the field is confined within a tube with constant cross section  $A$ , and that the contribution from the bag pressure

or confining currents is neglected <sup>7</sup>. The field energy per unit length is then given by  $\frac{1}{2}A\mathcal{E}^2 = \frac{1}{2}Q\mathcal{E}$ . We here used that the total flux,  $A\mathcal{E}$ , is determined by the charge  $Q$  spanning the rope. When a pair with elementary charge  $g/2$  is produced, the field is reduced to  $\mathcal{E} - \epsilon$ , where  $g/2 = A\epsilon$  is the flux from the elementary charge  $g/2$ . (The factor  $1/2$  is due to the conventional definition of  $g$ .) Neglecting the contribution to the tension from the bag pressure, and assuming that  $A$  is not modified, we obtain the “effective string tension” from the difference in field energy:

$$\tilde{\kappa} = \frac{1}{2}A\{\mathcal{E}^2 - (\mathcal{E} - \epsilon)^2\} = A\epsilon(\mathcal{E} - \epsilon/2) = \frac{1}{2}g(\mathcal{E} - \epsilon/2) \quad (3.5)$$

For a classical macroscopic field  $\mathcal{E}$ , the term  $\epsilon/2$  can be neglected in the parenthesis ( $\mathcal{E} - \epsilon/2$ ), and the expression in eq. (3.5) therefore looks like eq. (2.1). A problem shows up, however, if this formula is used to relate the effective string tension to the tension in an elementary string. Here the term  $-\epsilon/2$  can not be neglected, and it corresponds to the correction to the string tension due to the field produced by the new pair, as pointed out in ref. [31]. Taking this into account we get for an elementary string, with  $\mathcal{E} = \epsilon$ , the tension  $\kappa = g\epsilon/4$ , and the result

$$\tilde{\kappa} = (2p - 1)\kappa. \quad (3.6)$$

We note that for strong ropes, *i.e.* large values of  $p$ , this result is a factor 4 larger than the result in eq. (3.4). Here a factor 2 comes from the correction term in the elementary string, and another factor 2 is due to the relatively slow increase of the rope tension in eq. (3.3) for large  $p$ .

### 3.3.2 Particle multiplicity

For a rope stretched by  $(m + n)$  random colour charges, the rope can break up totally by only  $(p + q)$   $q\bar{q}$  pairs. The random walk in colour space here gives  $p + q \sim \sqrt{m + n}$  (see figure 3), and this effect therefore contributes to a reduction in the density of produced particles. In many references it is assumed that this is the dominant effect determining the multiplicity. Lacking a physical picture, it is often assumed that the hadrons are produced with the same separation in rapidity, see *e.g.* refs. [3, 5, 8].

Andersson and Henning [7] argue, however, that the early breakup can give a large energy to the leading particle(s), leaving less energy to produce softer particles. Amelin *et al.* [10] also argue that, as the breakups according to eq. (2.6) occur earlier for a stronger tension, the multiplicity should be lower. The arguments in refs. [7, 10] do, however not take into account that not only the space-time distance between breakup points becomes smaller for a higher effective string tension; also the size of the string pieces making up a hadron becomes smaller with the same scale factor. Therefore we argued in section 2.4.2 that the early breakup only gives a minor correction to the multiplicity, owing to the increased production of strange quarks (also admitting that unknown effects could influence the possibility for a  $q\bar{q}$  pair to fit into a final state hadron in case of a stronger effective string tension). Thus in our approach, the dominant effect on the total multiplicity is due to the random walk in colour space discussed above.

---

<sup>7</sup>In some cases the transverse area is taken as an undetermined parameter, *e.g.* in refs. [4, 7].

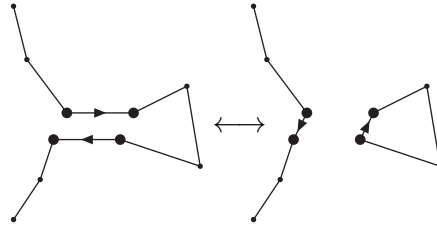


**Figure 4:** Sketch of how the initial state swing could reconnect colours between two dipoles in impact parameter space.

#### 4. Implementation of ropes in the DIPSY Generator

The rope model outlined above has been implemented in the DIPSY [15, 16, 59, 60] event generator. DIPSY is based on Mueller’s dipole cascade model [39–41], which is a formulation of leading-log BFKL evolution [61, 62] in transverse coordinate space, making it very well suited for a study of coherence effects based on spatial overlap of strings.

The DIPSY model introduces many sub-leading effects to Mueller’s dipole model (see appendix A for an introduction to the DIPSY model). Important to emphasize here is the initial state “swing”, which is a finite  $N_c$  effect. Two dipoles with the same colour form a colour quadrupole, where the colour field is better approximated by dipoles formed by the closest charge–anticharge pairs (*c.f.* figure 4). As smaller dipoles have smaller cross sections, this effect contributes to the saturation at small  $x$ .

By introducing saturation in the cascade using the colour swing, saturation directly becomes a finite- $N_c$  effect, as the effect obviously vanishes in the large- $N_c$  approximation. In section 4.1 we will argue how adding a similar reconnection effect in the final-state cascade, is a convenient way to introduce the singlet from the  $\mathbf{3} \otimes \bar{\mathbf{3}} = \mathbf{8} \oplus \mathbf{1}$  decomposition.

The gluons produced in the initial state in DIPSY are in the end ordered in both positive and negative light-cone momenta, and are allowed to continue radiating final-state bremsstrahlung according to the time-like dipole radiation model in momentum space [63, 64] implemented in the ARIADNE program [65]. Before forming the ropes, which will be sent to PYTHIA8 [66] for hadronization as described in section 4.2, the strings may also reconnect via a “final state swing” between dipoles with identical colours. This is introduced to account for the singlet from the  $3 \otimes \bar{3} = 8 \oplus 1$  decomposition of interacting string colours, and described in more details in section 4.1.

##### 4.1 The Final-state Swing

The swing mechanism was inspired by the colour reconnection mechanism proposed in [67] for the time-like dipole shower in ARIADNE [65]. The need for colour reconnections in the final state had already been noted in the context of multiple interactions [68]. Several other investigations were performed in the eighties and nineties looking at recoupling effects both in  $e^+e^-$ , DIS and hadronic collisions, see *e.g.* [69–72].

These reconnection models were based on the principle of minimizing “effective string lengths”. This was inspired by the string fragmentation, where the string action is given





**Figure 5:** Sketch of how the final state-swing could reconnect colours between two dipoles in momentum space.

by the area law for the Wilson loop [49]. For a simple  $q\bar{q}$ -string, which does not break, the action for one period is proportional to the total invariant squared mass  $s$ . For a string which breaks up into hadrons, the string area is instead proportional to  $\ln(s/m_0^2)$ , where the scale parameter  $m_0$  is a typical hadronic scale,  $\sim 1$  GeV. This area also determines the average hadron multiplicity. For a more complicated string configuration it is also possible to generalize this area to the so-called *lambda*-measure [73, 74]. The lambda-measure is infrared stable, but in cases without soft or collinear gluons, it can be approximated by

$$\lambda_s \propto \sum_{i=1}^{n-1} \ln \frac{(p_i + p_{i+1})^2}{m_0^2}. \quad (4.1)$$

Hence, when looking at the re-coupling of individual dipoles in a string it seems natural to try to minimise the sum of the logarithms of the dipole masses, or equivalently, the product of dipole masses.

In the original implementation in ARIADNE, only reconnections which decreased the total  $\lambda_s$  were allowed, but now we have reimplemented it in a way very similar to the swing in DIPSY. Between every final-state dipole radiation there is a possibility to recouple two dipoles,  $(12)(34) \rightarrow (14)(32)$ , if they are in the same colour state (using the same colour indices as in DIPSY). Again we treat emission and swing as competing processes, and while the emission of a gluon is simply given by the dipole formula

$$\frac{d\mathcal{P}_g}{d\rho} \approx dy \frac{C_F \alpha_S}{2\pi} \quad (4.2)$$

(for a  $q\bar{q}$ - dipole. For a gluon dipole  $C_F \mapsto C_A/2$ ). Here  $\rho = \ln(p_\perp^2)$  is the evolution parameter. We define the relative probability for the swing as

$$\frac{d\mathcal{P}_s}{d\rho} = \lambda \frac{(\mathbf{p}_1 + \mathbf{p}_2)^2 (\mathbf{p}_3 + \mathbf{p}_4)^2}{(\mathbf{p}_1 + \mathbf{p}_4)^2 (\mathbf{p}_3 + \mathbf{p}_2)^2}, \quad (4.3)$$

with a free parameter  $\lambda$  governing the relative strength of the swing.

Dipoles spanning large distances in impact parameter space are heavily suppressed in DIPSY due to the confinement effects imposed by the introduction of a small gluon mass,  $m_g$  (see appendix A). Even though the final-state swing in eq. (4.3) is formulated in momentum space and does not take into account any impact parameter dependence we

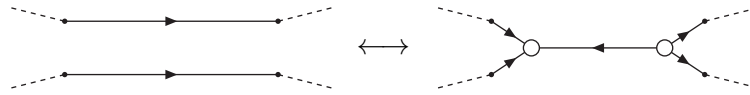


**Figure 6:** Sketch of how an antitriplet swing could reconnect colours between two dipoles by introducing two string junctions (denoted by circles).

still need to preserve these confinement effects. This is done by only considering dipoles which are closer in impact parameter space than a distance  $\propto 1/m_g$  as candidates for a swing.

It is interesting to note that if we have two completely anti-parallel dipoles, the probability of them having the same colour index is simply  $1/N_c^2$ , and if this is so, they will always reconnect, effectively breaking the “rope”. This corresponds to the singlet term which arises when combining the triplet and anti-triplet string,  $\mathbf{3} \otimes \bar{\mathbf{3}} = \mathbf{8} \oplus \mathbf{1}$  (see eq. (B.2)). This means that this effect in principle has already been taken care of before the formation of the rope, and when we later perform the random walk in colour space for overlapping strings, we need to constrain it to take this into account.

One could also imagine introducing another swing mechanism for the case of parallel strings, which would then imply that two (parallel) dipoles could swing into a single string according to the sketch in figure 6. This would involve the formation of two so-called *junctions* where three colour lines join. Although there is a mechanism for hadronizing junction strings in PYTHIA8, it has some technical limitations<sup>8</sup>. Also, the treatment of radiation from junction topologies in ARIADNE requires additional work, and we will thus defer the treatment of this new kind of swing to a future paper. Instead we will treat the corresponding multiplet configurations in the rope model below.

#### 4.2 Estimates of overlap region

As discussed in more detail in appendix A, the DIPSY Monte Carlo describes two colliding parton cascades, producing colour-connected partons located in transverse coordinate space and rapidity. This is followed by final-state radiation in momentum space from ARIADNE together with colour reconnection by the final-state swing. The location in the transverse plane is the basis for the interaction between the strings and the formation of ropes. As described in section 2.4, we expect that the dominant effect of rope formation is an enhanced production of strangeness and baryons, and in this paper we concentrate on these effects.

In section 3 we discussed an ideal situation with strings or colour flux tubes, which overlap completely in transverse space, and interfere constructively or destructively to form

---

<sup>8</sup>While preparing this manuscript a slightly improved version of the junction fragmentation was implemented in PYTHIA together with a colour reconnection mechanism producing junctions in the way depicted in figure 6 [27].

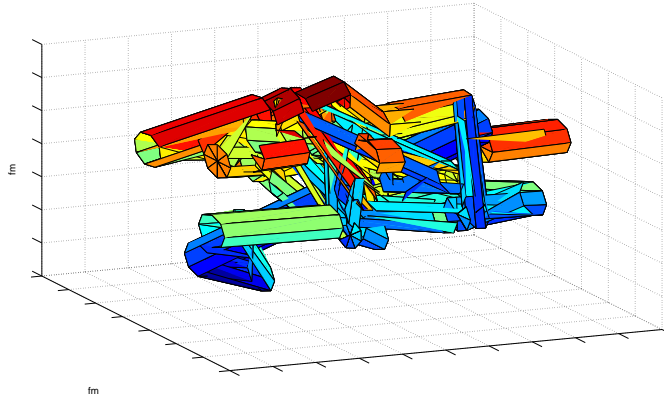


**Figure 7:** Illustration of strings from a  $pp$  event at  $\sqrt{s} = 7$  TeV in  $(\vec{b}_\perp, Y)$ -space before hadronization. Notice that the string radius is set at 0.1 fm – an order of magnitude less than in the calculation – in order to improve readability of the figure.

a coherent rope. A typical event, ready for hadronization, is shown in impact parameter space and rapidity in figure 7. The tubes in the figure represents colour connections between partons, and it is easy to see that real events are far from similar to the ideal situation, and we therefore need a way to estimate the amount of interaction. We naturally expect that strings close in transverse space should interfere more strongly than strings further away, with a typical interaction range of the order of the confinement scale. Our main assumption is therefore, that the degree of coherence between the strings is determined by the overlap between the corresponding flux tubes.

Since the DIPSY-generated events provide access to space-time information of strings, it is natural to alter the effect depending on the amount of overlap. Space-time information is usually not available in generators for  $pp$  collisions. It is, however, normally accesable in Molecular Dynamics Monte Carlo generators aimed for heavy ion collisions, where a similar approach (not including all fluctuations), has been studied in ref. [19]. We expect the coherence range (the radius of the flux tubes) to be of the order of the confinement scale, and put it to 1 fm. One could treat it as a completely free parameter, and tune it to data together with other free parameters, in order to give the most accurate description of data. Since neither the method of calculation of overlap between strings, nor the connection between this overlap and  $m$  and  $n$  (the number of uncorrelated colour and anticolour charges in one end of the rope) is obvious from first principles, we will present two different approaches for calculating the overlap. The first method is very crude, and approximates all strings as straight flux tubes (“pipes”) parallel to the rapidity axis. In this pipe-based approach, a string will be given values for  $m$  and  $n$  that are averages over the whole string, in fact an average over the full area in transverse space covered by the string. The string is subsequently hadronized with a single average value for  $\tilde{\kappa}$ , determined from  $m$  and  $n$  by the random walk procedure.

The second method is more detailed and takes into account more fluctuations along the string. In this dipole-based approach, a string is viewed as a chain of dipoles, connected by

gluons, either with quarks at the endpoints, or as closed gluonic loops. Overlaps are then calculated and a random walk in colour space is performed for each dipole, at a specific rapidity value, in order to change the value for  $\tilde{\kappa}$  at each breakup in the hadronization.

In both treatments the random walk is constrained to take into account that steps corresponding to  $\{1, 0\} \otimes \{0, 1\} \mapsto \{0, 0\}$  have already been treated in the final-state swing mechanism. Nevertheless it is clear that for  $m + n$  overlapping strings or dipoles, may end up in multiplets  $\{p, q\}$ , where  $p < m$  and/or  $q < n$ . This poses a problem, since for technical reasons, each of the  $n + m$  strings are hadronized separately, so we cannot break them with only  $p + q$  break-ups. Since the net effect is to reduce the multiplicity by a factor  $\propto (p + q)/(m + n)$ , we instead emulate this by simply randomly discarding strings in the pipe-based treatment with a probability  $1 - (p + q)/(m + n)$ . In the dipole-based treatment the approach is somewhat more sophisticated and we instead discard individual dipoles in a procedure inspired by the suggested *junction swing* in figure 6.

The details of the implementation of the two treatments are fairly technical and a full description is therefore deferred to appendices C.1 and C.2.

The aim of introducing two different approaches for calculating overlap, is to demonstrate that even the very crude pipe-based approach catches the gist of the model and improves the description of strangeness and baryon production, as described in section 5. Since further sophistication in the dipole-based approach can improve description of strange and baryonic content even further, we argue that a direct mapping from overlap in transverse space to  $m$  and  $n$  is indeed sensible. Further sophistication of this calculation of overlap is left for future publications.

### 4.3 Exclusive observables with DIPSY

The DIPSY Monte Carlo is implemented in the event generator framework called THEPEG [75]. Also the ARIADNE program for final-state parton showers has been implemented in this framework and there we have now added the final-state swing mechanism described in section 4.1. In THEPEG we have also written an interface to the hadronization routines of the PYTHIA8 event generator, and it is here we have implemented our rope hadronization models described in the previous section. The whole code is available from the authors upon request.<sup>9</sup>

The full code can generate full, exclusive final states for  $pp$ ,  $pA$  and  $AA$ . The goal driving event generators such as DIPSY is to be able to describe all collider physics with the same models, using the same parameters. As event generators in general have a quite large number of parameters, which parameterize the uncertainties in the models implemented, these parameters need to be estimated from data in a "tuning" process. It is important to state that tuning does not mean fitting of individual spectra to data. It rather means that one set of parameter values are estimated such that the same models can describe anything from  $e^+e^-$  over  $pp$  to  $pA$  and  $AA$  collisions.

We have already discussed some of the parameters on the Lund string fragmentation level, but there are many others, such as the non-perturbative cutoff in the parton cascade

---

<sup>9</sup>See also <http://home.thep.lu.se/DIPSY> for installation instructions.

and scale factors used in the running of  $\alpha_S$  (to emulate untreated higher orders). The tuning of these parameters is quite a complicated task, and for each event generator there are typically several different tunes available (see *e.g.* `mcplots.cern.ch` [76] for comparisons between different tunes of different programs).

The most common strategy is to first tune parameters associated with the final-state showers and hadronization to data from  $e^+e^-$  colliders. Assuming jet universality these are then fixed when tuning further parameters related to initial-state showers and multiple parton interactions to data from hadron colliders.

As we have tried to argue in this paper, the concept of jet universality is not quite straightforward, and the hadronization may very well behave differently in hadronic and  $e^+e^-$  collisions. To see the effects of our new model it is therefore necessary to take some care and make sure that the description of the flavour-dependent observables we wish to study is not dominated by a general change of multiplicity distributions for all particles, as such global effects would normally be removed in a tuning procedure. Therefore we have made a careful tuning both for the cases with rope effects and without, as detailed in appendix D.

Since the DIPSY event generator does not yet include a model for diffractive events, care also must be taken to only compare to observables that are not sensitive to diffraction. For that reason, we will primarily look at particle ratios. This point is also expanded upon in appendix D.

## 5. Results

In this section we will present some results from applying the introduced rope model. We will concentrate on flavour observables in minimum bias events in hadronic collisions in the energy range where we believe the small- $x$  approximation in the DIPSY model is valid,  $\sqrt{s} \gtrsim 100$  GeV. After presenting comparisons to experimental data in section 5.1, we will look at the model's sensitivity to parameters and its behaviour at higher energies in section 5.2. In section 5.3 we discuss the flow-like effects shown in the results.

### 5.1 Comparison to data

Results from DIPSY including the rope model in the dipole scheme (labelled 'Rope') are here compared to CMS data [36] at 900 and 7000 GeV as well as STAR data [77] at 200 GeV. We also show DIPSY with no rope effects on, labelled 'DIPSY', and finally a PYTHIA8 reference<sup>10</sup> labelled 'Pythia'. Comparison to data for more energies, and other kinematic variables *etc.* can be found on the project home page at <http://home.thep.lu.se/DIPSY/>. The parameters for rope hadronization used are  $r_0 = 1$  fm,  $\beta = 0.25$  and  $m_0 = 0.135$  GeV. These choices will be further discussed in section 5.2.

In figure 8 (left) we see the proton/pion ratio in bins of  $p_\perp$ , as measured by STAR, compared to simulations. We clearly see that DIPSY with no added effects fails to describe this ratio, in the same way as PYTHIA8 does. The proton/pion ratio is a good measure

---

<sup>10</sup>Version 8.180, tune 4C.

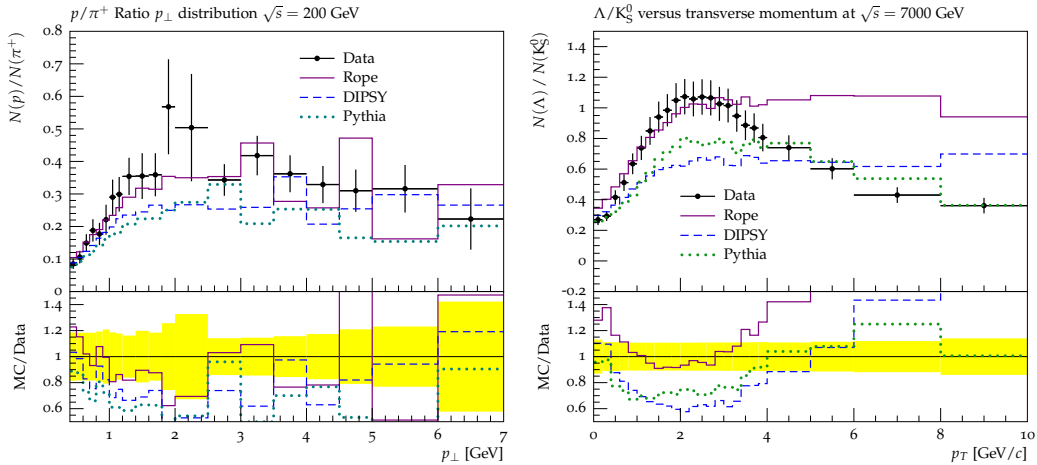


**Figure 8:** The proton to pion ratio in bins of  $p_{\perp}$  as measured by STAR at  $\sqrt{s} = 200$  GeV (left) and  $\Lambda/K_s^0$  at 7000 GeV as measured by CMS (right). Both results are compared to DIPSY with and without rope, as well as with PYTHIA8.

of the relative amount of baryons with no strangeness, governed by the  $\xi$ -parameter, and we see that DIPSY with added rope effects indeed describes data better, both in terms of relative proton content and  $p_{\perp}$ .

In figure 8 (right) the  $\Lambda/K_s^0$  ratio at  $\sqrt{s} = 7$  TeV is shown in bins of  $p_{\perp}$  as measured by CMS. As both the meson and the baryon has strangeness, this should also be a good measure of the influence of the  $\xi$ -parameter. We again see that including rope effects improves the description, especially in the low- $p_{\perp}$  end, where most of the multiplicity is concentrated. The high  $p_{\perp}$ -tail is poorly described, and we will discuss this further in section 5.3.

Figure 9 shows the  $\Lambda/K_s^0$  ratio at  $\sqrt{s} = 900$  GeV (left) and 7 TeV (right) in bins of rapidity as measured by CMS. We see here that the relatively weak dependence on energy is well described by the rope model, with the same values for  $r_0$ ,  $\beta$  and  $m_0$ .

The  $\Xi^-/\Lambda$  ratio is an observable, that is particularly sensitive to the  $\rho$  parameter. Figure 10 shows this ratio in bins of rapidity at 900 GeV and 7000 GeV, and we see that the rope model also reproduces the behaviour of these data fairly well.

Although the energy dependence shown in figures 9 and 10 is fairly weak, the fact that it is well described by the rope model is a very important point. At higher energies more strings are confined within a small space, and with the amount of overlap as a measure of the size of the rope effect, one could expect a larger increase with energy. To further illustrate this point, and to serve as qualitative predictions for the integrated particle ratios, we show in figure 11 the total  $K/\pi$ ,  $\Lambda/K_s^0$  and  $\Xi^-/\Lambda$  ratios as a function of  $\sqrt{s}$ . We note here that the combined effect of strangeness and baryon suppression is not factorizing in a simple way. As discussed in appendix C, the effects of an increased string tension is quite involved, especially for baryons. The fact that the relative abundances presented in figures 8-10 are well described, also for different energies, gives us confidence that our model has some physical relevance.

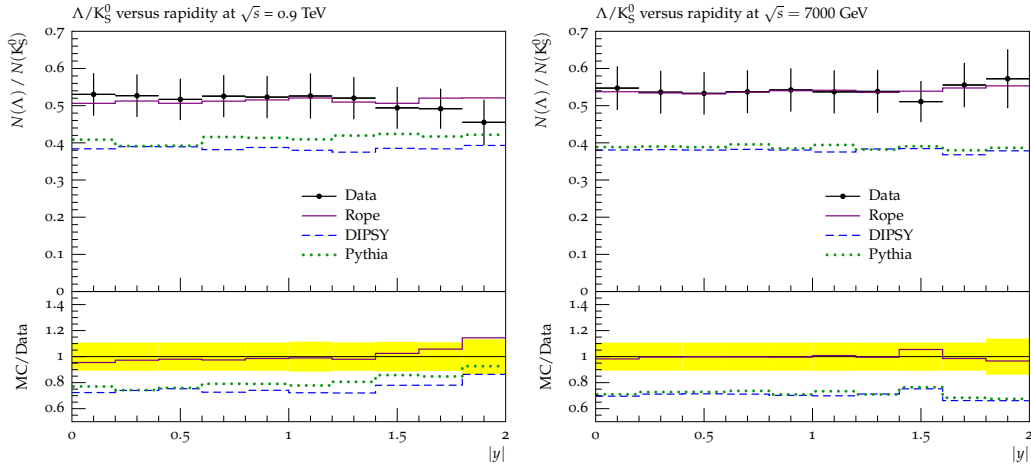


**Figure 9:** The  $\Lambda/K_s^0$  ratio at 900 GeV (left) and 7000 GeV (right) as measured by CMS in bins of rapidity. The figure shows that the rope model captures the (albeit weak) energy dependence of this ratio, while DIPSY without ropes, as well as PYTHIA8, shows no energy dependence.

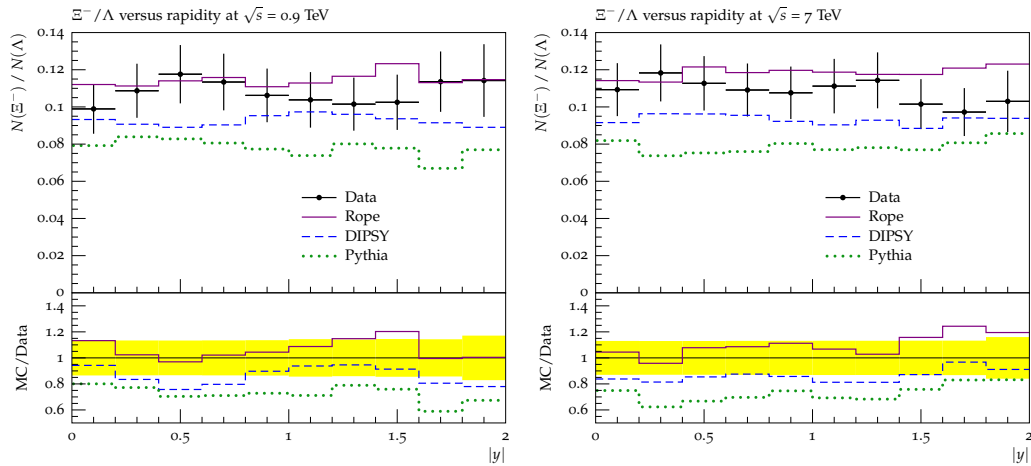


**Figure 10:** The ratio  $\Xi^-/\Lambda$  at 900 GeV (left) and 7000 GeV (right) as measured by CMS in bins of rapidity.

## 5.2 Model behaviour

The model introduces three new parameters. The string radius  $r_0$ , the popcorn-parameter  $\beta$ , and the parameter  $m_0$  which is specific to the dipole approach. The parameters have not been tuned to data in the usual sense, but set to reasonable physical estimates. We believe that the model in its current state is not mature enough to warrant a tuning, but one should nevertheless get an intuition for the uncertainties associated with the choice of parameters. We will here motivate our choices, and show the sensitivity of the model to changes in the parameter values, and how the results vary with  $\sqrt{s}$ .

To gauge the sensitivity we look at two quantities: the average string tension and the number of junctions. Focusing on particle ratios, we normalize to the  $\lambda$ -measure, which is a measure for the hadronic multiplicity (see eq. (4.1)). Thus we study the event averaged

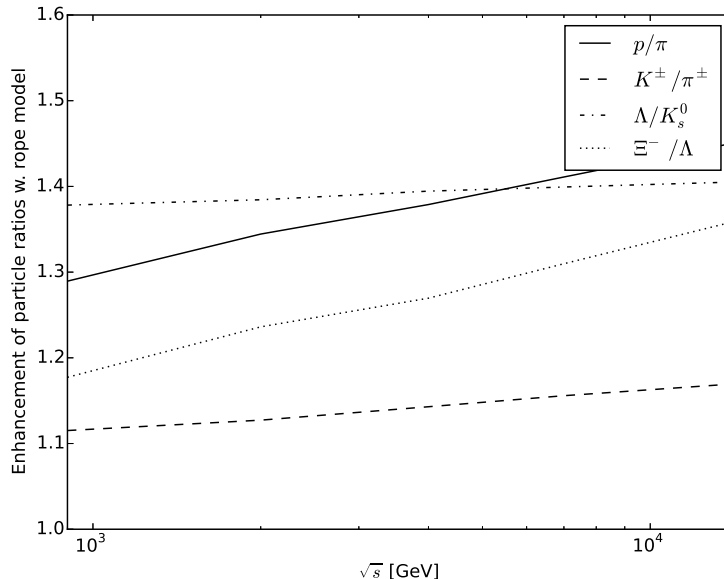


**Figure 11:** Enhancement of particle ratios of function of  $\sqrt{s}$ . Integrated ratios of  $p^\pm$  and  $K^\pm$  to  $\pi^\pm$ ,  $\Lambda\bar{\Lambda}$  to  $K_s^0$  and  $\Xi^-$  to  $\Lambda\bar{\Lambda}$  with the rope model (dipole approach) applied, normalized to the same ratio with ordinary string hadronization. All particles with  $p_\perp > 200$  MeV are included.

string tension, defined by the relation

$$\langle \tilde{\kappa}/\kappa \rangle \equiv \frac{\sum_i \lambda_i \tilde{\kappa}_i / \kappa}{\sum_i \lambda_i} \quad (5.1)$$

(where  $i$  counts all dipoles and  $\lambda_i = \ln(m_i^2/m_0^2)$ ), and the number of junctions per unit  $\lambda$ ,  $\langle n_j / \sum_i \lambda_i \rangle$ . These quantities can act as indicators for the amount of string overlap, which grows with increasing energy, but is also sensitive to the tunable parameters  $r_0$  and  $m_0$ .

Figure 12 (left) shows the average string tension as functions of  $\sqrt{s}$ , for  $r_0 = 1$  fm and  $m_0 = 0.135$  GeV. The dashed lines in figure 12 indicate the event-by-event fluctuations, showing one standard deviation. It is clearly visible that the enhancement effect rises logarithmically with  $\sqrt{s}$ . This is expected, as the number of gluons in the BFKL-based DIPSY cascade has the same energy dependence.

The average value of the string tension will thus increase with energy, and from figure 2 it is clear that this gives a larger amount of strange and baryonic activity as  $\sqrt{s}$  goes up, as well as having a moderate effect on total multiplicity due to the effect on the parameters  $a$  and  $b$  in the splitting function in eq. (2.5). However, the multiplicity in  $pp$  collisions are heavily influenced by the parameters controlling the initial-state evolution in DIPSY, and as described in appendix D, we tune these (while keeping the hadronization parameters tuned to LEP data fixed) to obtain the same multiplicity with and without rope effects. In this way the only effects from our rope model are the relative amounts of baryons and hadrons with a strange content; both are expected to increase.



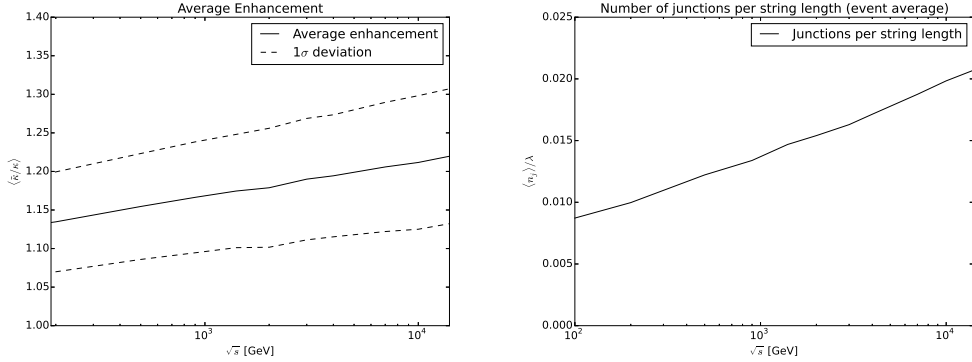


**Figure 12:** (left) Average enhancement  $\langle h \rangle = \langle \tilde{\kappa} / \kappa \rangle$  as a function of  $\sqrt{s}$  in  $pp$  collisions. The band indicates one standard deviation. (right) Number of junctions per string length as a function of  $\sqrt{s}$ .

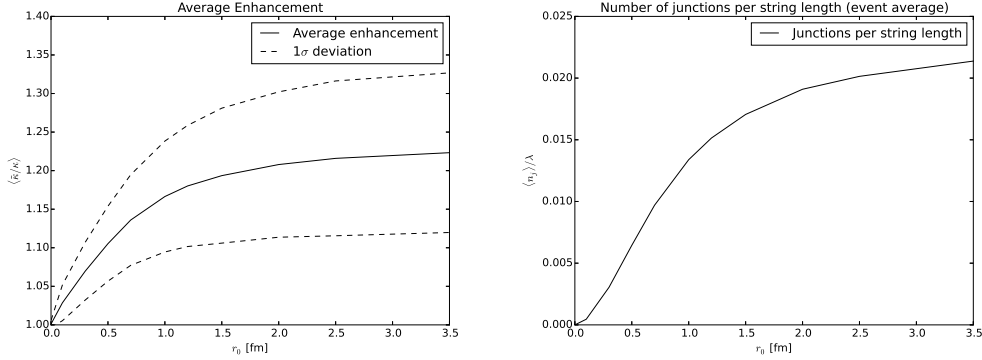


**Figure 13:** Average enhancement (left)  $\langle h \rangle = \langle \tilde{\kappa} / \kappa \rangle$  as a function of  $r_0$  at  $\sqrt{s} = 900$  GeV in  $pp$  collisions. The band indicates one standard deviation. Number of junctions (right) per string length as a function of  $r_0$ .

The increase in the number of junctions per string length is also shown in figure 12 (right). The amount of baryons emerging from the produced junctions is, as explained in appendix C.2, controlled by the popcorn strength parameter  $\beta$  (see eq. (C.5)). We note that while increasing  $\beta$  results in a stronger increase of baryons produced through diquark break-ups in the strings, it also decreases the probability that baryons are produced in junction structures, as explained in section C.2. As our results thus have very little sensitivity to variations in  $\beta$ , it is fixed to 0.25 throughout the article, and we do not expect large theoretical uncertainty to be ascribed to this parameter should the model be thoroughly tuned.

The amount of overlap in an event will also increase by increasing  $r_0$ . In figure 13 (left) the average enhancement is shown as a function of  $r_0$  at fixed energy  $\sqrt{s} = 900$  GeV and  $m_0 = 0.135$  GeV. It is interesting to note that the overlap saturates at  $r_0 \sim 1.5$  fm, as the size of the strings becomes larger than the proton. This behaviour is almost independent of collision energy, as the cross section only increases logarithmically with energy, although

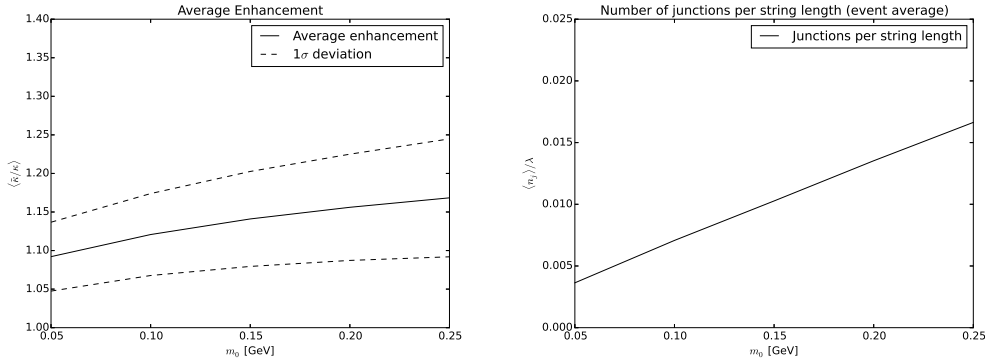


**Figure 14:** Average enhancement (left)  $\langle h \rangle = \langle \tilde{\kappa} / \kappa \rangle$  as a function of  $m_0$  at  $\sqrt{s} = 900$  GeV in  $pp$  collisions. The band indicates one standard deviation. Number of junctions (right) per string length as a function of  $r_0$ .

the value at saturation is higher for higher energies. The same type of saturation effect is found in the number of junctions, shown in figure 13 (right). Throughout the article,  $r_0$  is set to 1 fm, which is taken as a typical hadronic length scale. We expect variations in the parameter  $r_0$  to be the largest source of theoretical uncertainty should the model be tuned. In the region around  $r_0 \sim 1$  fm, small changes in  $r_0$  can give up to 5 % change in average effective string tension, which will of course be reflected in the results.

Finally the parameter  $m_0$  serves as a characteristic scale for the dipoles. This has both the effect of a cut-off in the rapidity span (gluons in a dipole at rest would otherwise give infinite rapidity), and as a propagation time ( $1/m_0$ ), to let the gluons propagate a finite distance (determined by their  $p_\perp$ ) before the overlap is calculated and hadronization takes place (see appendix C.2 for further explanation). The average enhancement factor and the density of junctions as function of  $m_0$ , is shown in figure 14.

The model is not as sensitive to  $m_0$  as to  $r_0$ , and we expect that the uncertainty after a tuning, which can be ascribed to  $m_0$ , will be only on the order of a few percent. In this article we have chosen to set the parameter  $m_0$  to the pion mass,  $m_0 = 0.135$  GeV, as no hadron can have a larger rapidity than the pion. The pion formation time will then be defining for the dipole propagation time. We believe that a tuning of this parameter will not give large deviations from the pion mass, as we have also tried hadronic scale  $1/r_0 \approx 0.2$  GeV. This is numerically close to the pion mass, but does not give an equally good energy dependence.

### 5.3 Particle ratios and flow-like effects

As seen, rope effects introduce a  $\sqrt{s}$ -dependence of flavour ratios and baryon ratios in the fragmentation, and we note in particular that the rise at small  $p_\perp$  is well described. This effect is often seen as an indication for the formation of a quark–gluon plasma phase, also in  $pp$ -collisions [78, 79], as the pressure in the hot plasma would push large mass particles to higher  $p_\perp$  (compared to low mass ones). In our rope model it is mainly the result of the colour reconnections induced by the final state swing mechanism, which originate from

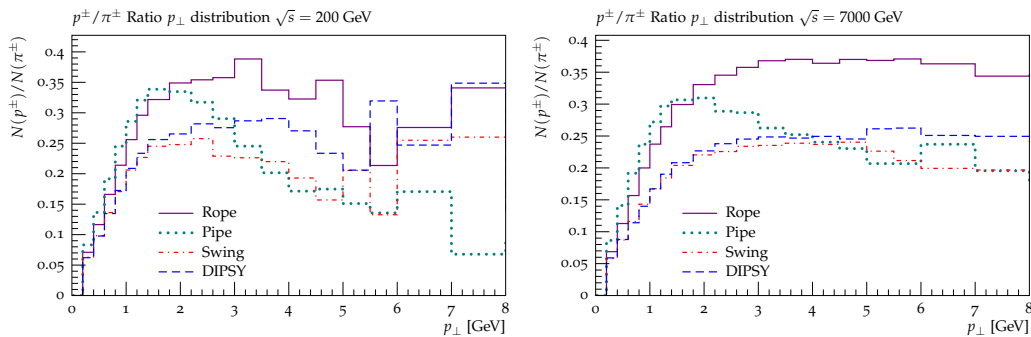


**Figure 15:** Proton ( $p + \bar{p}$ ) to pion ( $\pi^+ + \pi^-$ ) ratio in bins of  $p_\perp$  ( $|y| < 2.0$ ) at  $\sqrt{s} = 200$  GeV (left) and 7000 GeV (right).

the formation of lower colour multiplets. Ortiz *et al.* have previously noted that the colour reconnection model implemented in PYTHIA, gives rise to a flow-like effect in  $pp$  collisions at LHC [80].

It is also seen that, although the rise at small  $p_\perp$  is well described, the experimentally observed fall at higher  $p_\perp$ , in *e.g.*  $\Lambda/K_s^0$  shown in figure 8, is not reproduced by the present implementation of rope effects. In studies of plasma effects the hadrons with larger  $p_\perp$  are expected to originate from high- $p_\perp$  jets fragmenting outside the plasma (see *e.g.* ref. [78]). Such an effect should also be expected in the rope picture, where high- $p_\perp$  gluons are expected to hadronize outside the region where strings interfere, illustrated in figure 7. This effect is, however, not taken into account in the present implementation.

As a means to approximately account for the reduced rope effect for high- $p_\perp$  jets, we have studied a modified version of the “pipe” implementation described in appendix C.1. Here, in case any parton in the string, or any hadron arising from the string, obeys the criteria  $|y| < 2.0$  and  $p_\perp > 4$  GeV, the string will not feel any enhancement, but be hadronized with  $\tilde{\kappa}/\kappa = 1$ . As this happens in only a small fraction of the events, we believe that this crude measure gives a qualitatively correct estimate of the effect.

In figure 15 we show the  $p^\pm/\pi^\pm$  ratio at  $\sqrt{s} = 200$  and 7000 GeV. The curve marked ‘DIPSY’ shows simulation with no rope effects, but as the final state swing (labelled ‘Swing’) is added, we already see how the high- $p_\perp$  tail of the ratio distribution (at both energies) falls off a bit. Adding all rope effects (labelled ‘Rope’), we see how the integrated ratio increases (as shown before), but since the major effect on  $p_\perp$ , in the rope model, comes from the final state swing, the shape is not altered much. The curve labelled ‘Pipe’ shows the modified pipe-based approach to estimate the overlap, as discussed above. We see that in this version the high- $p_\perp$  tails are more suppressed, thus following the data better. The ‘Pipe’-curves also show that the ratios for low to intermediate  $p_\perp$  (where most of the multiplicity is) is affected roughly as expected, even with this very simple way of counting overlap<sup>11</sup>. The fact that even a simple treatment like the pipe based one can catch the gist of the rope model, is an encouraging indication that the interesting physics lies in the model

<sup>11</sup>We remind the reader that not even additional junctions are added in the ‘Pipe’-approach, all is due to changes in the  $\xi$  parameter.

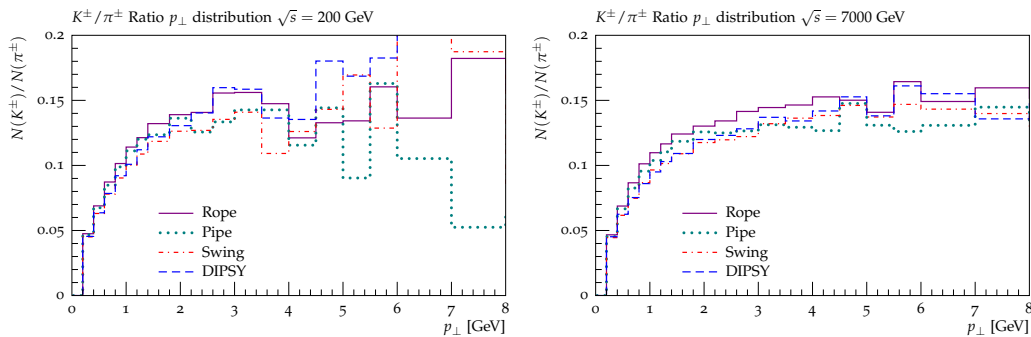


**Figure 16:** Kaon ( $K^+ + K^-$ ) to pion ( $\pi^+ + \pi^-$ ) ratio in bins of  $p_\perp$  at  $\sqrt{s} = 200$  GeV (left) and 7000 GeV (right).

itself, and not in a more or less arbitrary choice of how to estimate the numbers  $m$  and  $n$  denoting the number of interacting strings. We do, however, see that the  $\sqrt{s}$ -dependence for the pipe based approach is not nearly as good as the dipole based one. For this reason, we believe the dipole approach to bear more physical sense, and in sections 5.1 and 5.2, we have thus only shown the dipole approach.

In a future work we will address the issue of the high- $p_\perp$  tails in ratios. A more sophisticated version of the cut applied to the pipe based approach must be added to ensure that hadronization takes place with local parameters suitable for the actual location of the process, and not just let the dipoles propagate a fixed length.

In figure 16 we see the  $K^\pm/\pi^\pm$  ratio in bins of  $p_\perp$  at  $\sqrt{s} = 200$  GeV and 7000 GeV. This ratio does not show the same type of intermediate- $p_\perp$  "bump" (also not present in data, see *e.g.* ref. [81]), but rather a more smooth rise. The rope model (in both dipole and pipe approaches) shows some, but not much, effect, in accordance with our expectations.

## 6. Conclusions and outlook

It was early observed that string hadronization models, when tuned to  $e^+e^-$  annihilation data at LEP, underestimates the production of strange quarks in  $pp$  collisions. At the higher LHC energies the experiments show significantly enhanced production of strangeness and baryons, in particular strange baryons are strongly enhanced. In  $pp$  collisions the strings or cluster chains are usually assumed to hadronize independently, although the density of strings becomes quite high at LHC energies, and interaction between the strings therefore ought to be expected. Interaction between strings have been discussed by many authors in connection with nucleus collisions, where very high string densities are also expected. Here the formation of "ropes" are generally predicted to give higher ratios of strange particles and baryons. Although the geometrical distribution of nucleons within a nucleus can give a good estimate of the density of strings in nucleus collisions, for a quantitative description of string interaction in  $pp$  collisions, a description of the parton distribution in impact parameter space must be essential.

In this work we use the DIPSY model, which is a formulation of BFKL evolution in transverse coordinate space, including NLL effects and effects of saturation and confinement,

taking also fluctuations and correlations into account. Within this model it is possible to calculate the distribution of strings in the transverse plane, and thus estimate the amount of interaction. For the actual hadronization process we use PYTHIA8.

Following the early work by Biro *et al.* [3], we assume that a set of strings within a limited transverse size can interact coherently, forming a colour rope. If the strings are stretched between random colour charges, the net charge at the end of a rope is obtained by a random walk in colour space. Results from lattice calculations show that the tension in a rope is proportional to the corresponding quadratic Casimir operator. If the rope breaks up in a step-wise manner by the production of  $q\bar{q}$  pairs, then the number of such pairs needed to break the rope, is in general smaller than the initial number of strings. More energy will, however, be released in the production of the individual pairs, thus simulating a higher effective string tension. An important point is here that it is the decrease in rope tension following the  $q\bar{q}$  pair production, which specifies the “effective string tension”, and we note here that this leads to a significantly smaller increase, compared to what is usually assumed.

Besides higher fractions of strange particles and baryons, a higher string tension also implies that the string breaks earlier. Early breakups usually imply lower multiplicity, but we argue here that for rope hadronization this effect is compensated by the fact that shorter string pieces are needed to form a final state hadron.

Special attention is needed for handling colour singlets, which can be formed *e.g.* when a triplet and an antitriplet combines as  $\mathbf{3} \otimes \bar{\mathbf{3}} = \mathbf{8} \oplus \mathbf{1}$ . We treat this by colour reconnection via a “final state swing”, described in section 4.1. This idea could potentially also be used to reconnect parallel strings into the anti-triplet in  $\mathbf{3} \otimes \mathbf{3} = \mathbf{6} \oplus \bar{\mathbf{3}}$  (see eq. (B.1)), as sketched in figure 6. As the hadronization model in PYTHIA8 is currently being improved to better handle complicated junction topologies, we expect to be able to implement such a sextet swing mechanism in ARIADNE in the near future.

Naturally the range within which the strings can act coherently cannot be calculated from basic principles. It ought to be of the hadronic scale  $\sim 1$  fm, but might be treated as a tunable parameter. Partly overlapping strings also give rise to uncertainties. We have here studied two different schemes for estimating the effects of rope formation, which both attempt to account for the actual overlap of strings in impact parameter space and rapidity. The schemes differ in the level of detail considered; the “pipe-based” scheme is only looking at the average enhancement of the tension in a string, while the “dipole-based” version estimates the increased string tension in each individual string break-up. The dipole scheme also introduces a simple junction model, both formation and breaking. In spite of the differences between the schemes, the results are fairly similar. In both cases observables sensitive to the increased relative abundance of baryons and strange hadrons are much better described by the rope models, compared to conventional string fragmentation.

The fact that the model reproduces the increase both for several collision energies and for several different hadron species, is a strong indication that our picture of the increased string tension in overlapping strings, and its effect on the fragmentation process, is reasonable. Although our model introduces a couple of new parameters, we have shown that these mainly affects the overall strength of the effect, while the influence of the string

tension on individual hadron species is fixed by the model and by the tuning of parameters in PYTHIA8 to single-string data from  $e^+e^-$ -experiments. Also the energy dependence is fairly well constrained by the comparison to data presented in this article, and our implementation in the DIPSY generator can therefore make rather firm predictions, *e.g.* for relevant observables to be measured at Run 2 of the LHC.

A particularly interesting result is that the model reproduces the increase in the ratios  $p/\pi$  and  $\Lambda/K$  with  $p_\perp$  in the range  $p_\perp < 2$  GeV, in a way mimicking a hydrodynamic transverse flow. This effect is frequently interpreted as caused by a transition to a quark–gluon plasma. It was also pointed out in ref. [80] that colour reconnection, as implemented in PYTHIA, gives rise to a flow-like effect in  $pp$  collisions. Thus the results presented in section 5 originate partly from the increased tension in ropes with high colour multiplets, and partly from colour reconnections in cases where strings combine to colour singlets or other small multiplets.

Our model does, however, not reproduce the drop in the  $p/\pi$  ratio for  $p_\perp > 2$  GeV. In analyses based on flow, it is frequently assumed that high- $p_\perp$  particles result from fragmentation of jets not participating in the thermalisation, and hadronizing outside the plasma (see *e.g.* ref. [78]). A similar effect should be expected in our rope model. High- $p_\perp$  hadrons may be predominantly formed outside the overlap regions, and therefore not feel the increased tension in the rope. This effect is not included in the present implementation of the model, giving the results presented in section 5. A crude modification of our pipe-based scheme indicates that the effect may be qualitatively accounted for, but further studies are needed of the formation times and the transverse propagation in space within our rope model. In this context we also need to revisit the description of high- $p_\perp$  gluons, which currently are not well modelled in DIPSY.

We have in our analyses also neglected a possibly increased pressure exerted by the ropes. In the bag model the pressure from a high colour flux tends to expand the transverse size of a flux tube, in a way which also could contribute to flow-like effects. An estimate of this effect also needs a better understanding of the relative time-scales for rope formation and the hadronization process.

We conclude that several mechanisms can contribute to the flow-like behaviour in high energy collisions: besides a phase transition to a plasma, also increased string tension in colour ropes, colour reconnection in low colour multiplets, and transverse expansion due to high pressure inside the ropes. To estimate the relative contributions from these sources, it is important to study different reactions,  $pp$ ,  $pA$ , and  $AA$ , and also all possible observables, besides those discussed in this paper also *e.g.* angular flow, fluctuations, and correlations of different kinds. The time-scales for the different processes is here very important. We want to return with results of such studies in forthcoming publications.

## Acknowledgments

Work supported in part by the MCnetITN FP7 Marie Curie Initial Training Network, contract PITN-GA-2012-315877, the Swedish Research Council (contracts 621-2012-2283

and 621-2013-4287), and contract DE-AC05-06OR23177 under which the Jefferson Science Associates, LLC operate the Thomas Jefferson National Accelerator Facility.

## A. The DIPSY model

It has since long been clear that a proper description of the multi-particle final states in high energy hadron collisions requires some kind of multi-parton interaction model. The most successful such model to date is the one developed by Sjöstrand and van Zijl [68], but also other models have been proposed (see *e.g.* [82] and [83]).

For the purpose of our investigations, however, it is important that not only the momentum distribution of the produced partons is described; to estimate the degree to which strings overlap we also need to understand the impact-parameter distribution of partons. For this reason we have used DIPSY event generator [16], which will be described briefly in this appendix.

DIPSY is based on Mueller’s dipole cascade model [39–41], which is a formulation of leading-log BFKL evolution [61, 62] in transverse coordinate space. This model relies on the fact that initial-state radiation from a colour charge (quark or a gluon) in a hadron is screened at large transverse distances by an accompanying anticharge, and that gluon emissions therefore can be described in terms of colour-dipole radiation. Thus the partonic state is described in terms of dipoles in impact-parameter space and rapidity, which is evolved in rapidity when an emitted gluon splits a dipole into two. We here note that the suppression of large dipoles in transverse coordinate space is equivalent to the suppression of small  $k_\perp$  in the conventional BFKL evolution in momentum space.

For a dipole with charges at the transverse points  $\mathbf{x}_1$  and  $\mathbf{x}_2$ , the probability to emit a gluon at  $\mathbf{x}_g$  is given by

$$\frac{d\mathcal{P}_g}{dY} = \frac{\bar{\alpha}}{2\pi} d^2\mathbf{x}_g \frac{(\mathbf{x}_1 - \mathbf{x}_2)^2}{(\mathbf{x}_1 - \mathbf{x}_g)^2(\mathbf{x}_g - \mathbf{x}_2)^2}, \quad \text{with } \bar{\alpha} = \frac{N_c\alpha_s}{\pi}. \quad (\text{A.1})$$

The emission produces two new dipoles,  $(\mathbf{x}_1, \mathbf{x}_g)$  and  $(\mathbf{x}_g, \mathbf{x}_2)$ , which can split independently by further gluon emissions. Repeated emissions form a cascade, with dipoles connected in a chain. When two cascades collide, a dipole  $(\mathbf{x}_1, \mathbf{x}_2)$  in a right-moving cascade can interact with a left-moving dipole  $(\mathbf{x}_3, \mathbf{x}_4)$ , with probability

$$P = \frac{\alpha_s^2}{4} \left[ \ln \left( \frac{(\mathbf{x}_1 - \mathbf{x}_3)^2(\mathbf{x}_2 - \mathbf{x}_4)^2}{(\mathbf{x}_1 - \mathbf{x}_4)^2(\mathbf{x}_2 - \mathbf{x}_3)^2} \right) \right]^2. \quad (\text{A.2})$$

In a series of papers [15, 16, 59, 60] a generalization of Mueller’s model, implemented in the Monte Carlo event generator DIPSY, has been described in detail. Here we will only discuss the main points. The basic idea behind the model is to include important non-leading effects in the BFKL evolution, saturation effects in the evolution, and confinement.

The full next-to-leading logarithmic corrections have been calculated and have been found to be very large [84, 85]. A physical interpretation of these corrections has been presented by Salam [86], and a dominant part is related to energy–momentum conservation. In the DIPSY model this is achieved by equating the emission of a gluon at small transverse distances with high transverse momenta of the emitted and recoiling gluons. In this way the gluons emitted in the evolution are traced in both momentum and coordinate space, allowing us to generate the final-state momentum distribution of gluons. The conservation of



energy and momentum implies a dynamic cutoff for very small gluons with correspondingly high transverse momenta. This constraint has also important computational advantages; in the standard Mueller model the number of small gluons diverges which, although the cross section is still finite, gives computational problems.

Other important non-leading effects are the running coupling,  $\alpha_s(p_\perp^2)$ , and the “energy scale terms” (which correspond to the consistency constraint discussed by Kwiecinski et al. [87]). The latter implies that the emissions are ordered in both the positive and negative light-cone components [88]. Besides these perturbative corrections, confinement effects are included via a small gluon mass,  $m_g$ , and non-linear saturation effects through the so-called swing mechanism, described in more detail below.

In a high energy collision, two hadrons are evolved from their respective rest frames to a Lorentz frame in which they collide. In its own rest system a proton is currently modelled by a simple triangle of gluons connected by dipoles, and the gluonic Fock state is built by successive dipole emissions of virtual gluons. (The small- $x$  gluons are rather insensitive to the initial parton configuration, apart from the overall size, and valence quarks are later introduced by hand in the final state). The two evolved systems are then made to collide, allowing some of the dipoles in the left-moving system to interact with some in the right-moving ones. This enables the gluons in these dipoles to come on-shell, together with all parent dipoles, while non-interacting dipoles must be regarded as virtual and thus be reabsorbed.

### A.1 The initial-state Swing mechanism

The swing mechanism in DIPSY is a saturation effect within the evolution, which is conceptually interesting in connection with the rope formalism in this article. Mueller’s dipole evolution is derived in the large  $N_c$  limit, where each colour charge is uniquely connected to an anticharge within a dipole. Saturation effects are here included as a result of multiple dipole collisions, in the frame used for the analysis. Such multiple interactions give dipole chains forming loops, and are related to multiple pomeron exchange. Loops formed within the evolution are, however, not included.<sup>12</sup> Besides missing parts of the saturation, this also makes the result dependent on the frame used for the calculation. As dipole interaction in eq. (A.2) is colour suppressed compared to the dipole splitting, loop formation is related to the possibility that two dipoles have identical colours.

If two dipoles happen to have the same colour, we have actually a colour quadrupole, where a colour charge is effectively screened by the nearest anticolour charge. Thus approximating the field by a sum of two dipoles, one should preferentially combine a colour charge with a nearby anticharge. This interference effect is taken into account in DIPSY in an approximate way, by allowing two dipoles with the same colour to recouple forming the new dipoles, in a way that favours small dipoles.

In the simulation this is handled by assigning all dipoles a colour index running from 1 to  $N_c^2$ , not allowing two dipoles connected to the same gluon to have the same index. A pair

---

<sup>12</sup>This is also the case *e.g.* for the non-linear BK equation [89,90], which describes the interaction between a relatively dilute cascade and a dense target.

of two dipoles,  $(\mathbf{x}_1, \mathbf{x}_2)$  and  $(\mathbf{x}_3, \mathbf{x}_4)$ , with the same colour may be better approximated by the combination  $(\mathbf{x}_1, \mathbf{x}_4)$  and  $(\mathbf{x}_3, \mathbf{x}_2)$ , if these dipoles are smaller. In the evolution the pair is allowed to “swing” back and forth between the two possible configurations as indicated in figure 4. The swing mechanism is adjusted to give the relative probabilities

$$\frac{P_{(12)(34)}}{P_{(14)(32)}} = \frac{(\mathbf{x}_1 - \mathbf{x}_4)^2(\mathbf{x}_3 - \mathbf{x}_2)^2}{(\mathbf{x}_1 - \mathbf{x}_2)^2(\mathbf{x}_3 - \mathbf{x}_4)^2}, \quad (\text{A.3})$$

thus favouring the configuration with smallest dipoles. (In the implementation of the cascade evolution, the swing is competing with the gluon emission in eq. (A.1), where a Sudakov-veto algorithm can be used to choose which of the two happens next.)

The dipole interaction in eq. (A.2) is smaller for smaller dipoles, which reproduces the colour transparency effect. As the swing leads to smaller average dipole size, the probability for interactions is reduced, and thus the swing represents a saturation effect within the evolution. This reduced interaction probability is equivalent to the  $2 \rightarrow 1$  and  $2 \rightarrow 0$  vertices in *e.g.* the BK evolution equation.

## B. Colour algebra

### B.1 Calculation of $p$ and $q$

In this section the recursion relations presented in eq. (3.2) for calculating all possible  $\{p, q\}$  multiplets arising from the combination of  $m$  triplets and  $n$  antitriplets will be presented in detail.

It is worth noting that the combination of any SU(3) multiplets can be carried out using Young tableaux (just as the more familiar case of SU(2)). In the notation of this article, an SU(3) multiplet is denoted by the quantum numbers  $p$  and  $q$ , which can be directly a Young tableaux, as  $\{1, 0\} = \square$  and  $\{0, 1\} = \overline{\square}$ , and so the number of boxes in the top row is  $p + q$ . and the number of boxes in the bottom row is  $q$ .

Now the usual rules of manipulating Young tableaux can be used to review the simple cases of combining a single triplet with an (anti-)triplet:

$$\{1, 0\} \otimes \{1, 0\} = \square \otimes \square = \square\square \oplus \overline{\square} = \{2, 0\} \oplus \{0, 1\}, \quad (\text{B.1})$$

$$\{1, 0\} \otimes \{0, 1\} = \square \otimes \overline{\square} = \overline{\square\square} \oplus I = \{1, 1\} \oplus \{0, 0\}, \quad (\text{B.2})$$

where  $I = \{0, 0\}$  denotes a singlet. Note that symmetry ensures that  $\{1, 0\} \otimes \{1, 0\} = \{0, 1\} \otimes \{0, 1\}$ . Physically eq. (B.1) corresponds to the situation where two colour strings, with colour flow in the same direction, merge to a rope. In the case where the colour pairs are equal, the resulting rope will be a sextet ( $\{2, 0\}$ ), and in all other cases an antitriplet ( $\{0, 1\}$ ). Eq. (B.2) corresponds to two strings with opposite colour flow merging. This can either result in a gluon-like octet rope ( $\{1, 1\}$ ) or no colour flow at all, in the singlet case.

The recursion relations of eq. (3.2) can be derived using a similar procedure. Adding a single triplet to an existing multiplet  $\{p, q\}$  gives eq. (3.2) directly, as:

$$\begin{aligned} \{p, q\} \otimes \{1, 0\} &= \underbrace{\overbrace{\square \oplus \dots \oplus \square}^q \dots \underbrace{\overbrace{\square \oplus \dots \oplus \square}^p \dots \square}_p}_{q \oplus p} \otimes \square = \\ &\{p, q - 1\} \oplus \{p - 1, q + 1\} \oplus \{p + 1, q\}. \end{aligned} \quad (\text{B.3})$$

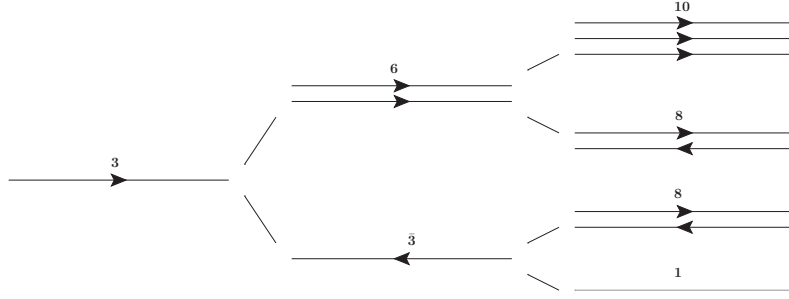


**Figure 17:** Illustration of the addition of triplets to an initial triplets, reads from left to right. By combining the initial  $\mathbf{3}$  in the left column with another  $\mathbf{3}$ , one gets either  $\mathbf{6}$  or  $\bar{\mathbf{3}}$  and so on (see text).

Combining the general  $\{p, q\}$  multiplet with an antitriplet proves directly symmetry is ensured as:

$$\begin{aligned} \{p, q\} \otimes \{0, 1\} &= \underbrace{\begin{array}{|c|c|} \hline \square & \square \\ \hline \end{array}}_q \cdots \underbrace{\begin{array}{|c|c|} \hline \square & \square \\ \hline \end{array}}_p \otimes \begin{array}{|c|} \hline \square \\ \hline \end{array} & \text{(B.4)} \\ &= \{p-1, q\} \oplus \{p, q+1\} \oplus \{p+1, q-1\}. \end{aligned}$$

Using the stated recursion relations, a random walk in colour space is simulated, as in ref. [3] by starting from a singlet  $I = \{0, 0\}$ . The resultant relation between  $\langle p+q \rangle$  and  $m+n$  is shown in figure 3.

In the same way the recursion relation for all multiplets arising from combining the general  $\{p, q\}$  multiplet with an octet can be defined. The proof follows in a straightforward way from the same considerations as above, and only the result is stated here:

$$\begin{aligned} \{p, q\} \otimes \{1, 1\} &= \{p-1, q-1\} \oplus \{p+1, q+1\} \oplus 2 \cdot \{p, q\} \oplus \{p-1, q+2\} & \text{(B.5)} \\ &\oplus \{p+1, q-2\} \oplus \{p-2, q+1\} \oplus \{p+2, q-1\}. \end{aligned}$$

## B.2 An illustrative example

As a simple illustrative example we can look at a rope spanned between three quarks with random colours in one end, matched by three antiquarks in the other end, illustrated in figure 17. The first quark is a triplet,  $\mathbf{3}$ , denoted  $\{1, 0\}$ , and depicted to the left in figure 17. The addition of a second quark can give a  $\mathbf{6}$  ( $\{2, 0\}$ ) or an  $\bar{\mathbf{3}}$  ( $\{0, 1\}$ ), as shown in the central column of figure 17, with probabilities  $2/3$  and  $1/3$  respectively. Adding the third quark to the sextet can give  $\mathbf{10}$  ( $\{3, 0\}$ ) or  $\mathbf{8}$  ( $\{1, 1\}$ ), while adding it to the  $\bar{\mathbf{3}}$  gives  $\mathbf{8}$  ( $\{1, 1\}$ ) or a singlet ( $\{0, 0\}$ ), as shown in the rightmost column in figure 17. The result is therefore a decuplet, two octets, and a singlet, with probabilities proportional to their respective multiplicities (*i.e.*  $10/27$ ,  $8/27$ ,  $8/27$ , and  $1/27$ ).

For the fragmentation of the rope, we find first that in the case of the singlet, there is no colour field stretched. For the decuplet and the octets the relative rope tension is  $9/2$  and  $9/4$  respectively. The decuplet can fragment in three steps giving successively a sextet

and a triplet, before the final breakup. The relative effective string tension,  $\tilde{\kappa}/\kappa$ , in these steps are  $9/2 - 5/2 = 2$ ,  $5/2 - 1 = 3/2$ , and 1 respectively. Thus the first breakup will give the highest effective string tension, and correspondingly higher  $s/u$ -ratio and higher  $p_{\perp}$ . An initial octet will similarly break in two steps via a triplet, with  $\tilde{\kappa}/\kappa$  equal to  $9/4 - 1 = 5/4$ , followed by the break of the triplet with the tension  $\kappa$  for a single string. If the  $\{p, q\}$  multiplet is in the left end of the rope, the antiquark is pulled to the left when  $p$  is reduced, and pulled to the right when  $q$  is reduced.

### C. Detailed description of the rope models

The models for rope formation and fragmentation presented in this paper are similar in spirit, but as always when implementing models in a Monte Carlo code, there are a number of choices to be made and different levels of detail that can be chosen. One of our models is fairly crude, using the average overlap for individual strings in an event, while the other is very detailed in the treatment of the individual string break-ups.

In common for the two models is that, for technical reasons, the fragmentation of a rope is done one individual string at the time, emulating the rope effects by modifying the parameters in the string fragmentation implementation of PYTHIA8, thus taking into account the effective string tension of the rope. We have concentrated on a selection of parameters which should be particularly sensitive to rope effects:

- $\rho$ : the suppression of  $s$  quark production relative to  $u$  or  $d$  type production.
- $\xi$ : the suppression of diquark production relative to quark production, meaning *(all diquarks)/(all quarks)*.
- $x$ : the suppression of diquarks with strange quark content relative to diquarks without strange quarks (in addition to the factor  $\rho$  for each extra  $s$ -quark).
- $y$ : the suppression of spin 1 diquarks relative to spin 0 diquarks (not counting a factor three due to the number of spin states of spin 1 diquarks).
- $\sigma$ : the width of the transverse momentum distribution in string break-ups.

Of these we assume that  $\rho$ ,  $x$  and  $y$  are directly related to mass effects in the tunneling mechanism in eq. (2.2), such that if the modification of the string tension be given by a simple scaling with an enhancement factor  $h$ , such that  $\kappa \mapsto \tilde{\kappa} = h\kappa$ , we obtain the following rescalings:

$$\begin{aligned}
 \rho &\mapsto \tilde{\rho} = \rho^{1/h}, \\
 x &\mapsto \tilde{x} = x^{1/h}, \\
 y &\mapsto \tilde{y} = y^{1/h}.
 \end{aligned}
 \tag{C.1}$$

Also the scaling of  $\sigma$  is quite straight forward and is simply given by  $\sigma \mapsto \tilde{\sigma} = \sigma\sqrt{h}$ .

The treatment of the  $\xi$  parameter is somewhat more involved as it gives a global probability of having a diquark break-up relative to a simple quark break-up, which means

it cannot be simply related to the tunneling mechanism. Looking at the relation between the individual probabilities for different quarks and diquarks, they are determined by the relations:  $\mathcal{P}_s = \rho\mathcal{P}_u$ ,  $\mathcal{P}_{ud_1} = 3y\mathcal{P}_{ud_0}$  and  $\mathcal{P}_{us_1} = x\rho\mathcal{P}_{ud_1}$ , *etc.* The total probability for diquark production relative to quark production, can therefore be expressed in terms of the ratio  $\mathcal{P}_{ud_0}/\mathcal{P}_u$ .

$$\xi \equiv \frac{\sum_{qq_s} \mathcal{P}_{qq_s}}{\sum_q \mathcal{P}_q} = \frac{1 + 2x\rho + 9y + 6x\rho y + 3yx^2\rho^2}{2 + \rho} \frac{\mathcal{P}_{ud_0}}{\mathcal{P}_u} \equiv \alpha \frac{\mathcal{P}_{ud_0}}{\mathcal{P}_u}, \quad (\text{C.2})$$

(where we have assumed that  $u$  and  $d$  quarks are equivalent).

However, it is not the case that  $\mathcal{P}_{ud_0}/\mathcal{P}_u$  is affected by the string tension in the same way as the  $\rho$ -parameter. According to the popcorn mechanism described in section 2.3 and figure 1, there is a two step procedure where first a  $q\bar{q}$  pair is produced as a fluctuation that does not break the string, and then another pair is produced which actually does, allowing a diquark–antidiquark pair to tunnel out. We will therefore assume that the ratio is composed of two factors, one is related to the probability to have a  $q\bar{q}$  fluctuation in the first place, and one related to the differences in masses. We will call these  $\beta$  and  $\gamma$  respectively, where we assume that  $\beta$  is independent of the string tension, while  $\gamma$  transforms as  $\rho$ .

Hence we have  $\xi = \alpha\beta\gamma$  where

$$\alpha \mapsto \tilde{\alpha} = \frac{1 + 2\tilde{x}\tilde{\rho} + 9\tilde{y} + 6\tilde{x}\tilde{\rho}\tilde{y} + 3\tilde{y}\tilde{x}^2\tilde{\rho}^2}{2 + \tilde{\rho}}, \quad (\text{C.3})$$

and

$$\gamma \mapsto \tilde{\gamma} = \gamma^{1/h}, \quad (\text{C.4})$$

and the total effect on  $\xi$  from a modified string tension is given by

$$\xi = \alpha\beta\gamma \mapsto \tilde{\xi} = \tilde{\alpha}\beta \left( \frac{\xi}{\alpha\beta} \right)^{1/h}. \quad (\text{C.5})$$

As explained in section 2.4.2, also the parameters  $a$  and  $b$  are indirectly affected by a modified string tension. One could also expect other parameters to be affected, but the ones presented here are the the most important ones.

### C.1 A pipe-based treatment

In the crude, pipe-based approach, we expect all flux tubes to be directed dominantly along the rapidity axis. For a string stretched from parton  $(\vec{b}_0, y_0)$ , via the gluons  $(\vec{b}_i, y_i)$ , and ending at  $(\vec{b}_k, y_k)$ , the volume of the corresponding flux tube in (*transverse coord.*, *rapidity*) space is thus given by

$$V_{string} = \sum_{i=1}^k \pi r_0^2 |y_i - y_{i-1}|. \quad (\text{C.6})$$

As the string can go back and forth in rapidity, the separations in rapidity enters with its absolute value. To estimate the amount of overlap between two strings, we must take into account that the string tubes are not parallel to the rapidity axis, but go up and down

in transverse space. This is approximated by replacing the winding flux tube by a wider straight pipe, with a correspondingly lower density. The pipe is parallel to the rapidity axis and stretched between the partons with the smallest and the largest rapidity,  $y_{min}$  and  $y_{max}$ . Its center is taken at  $\vec{b}_{cent} = (\vec{b}_{min} + \vec{b}_{max})/2$ , and its radius,  $r_{pipe}$ , is increased to enclose the major part of a wiggling string:

$$r_{pipe}^2 = r_0^2 + \frac{1}{k} \sum_{i=0}^k (\vec{b}_i - \vec{b}_{cent})^2. \quad (\text{C.7})$$

The volume of the pipe is thus given by  $V_{pipe} = \pi r_{pipe}^2 (y_{max} - y_{min})$ . Note that since the string can go back and forth, the ratio  $d = V_{string}/V_{pipe}$  can be larger than one. This number is the relative field density in the pipe, and in terms of overlap, it represents the string's ‘‘self-overlap’’. It is, however, important to keep track of the direction of the overlap. The relative field density in each pipe is thus assigned both an  $m$  and an  $n$  component, defined by the sign of its projection on the rapidity axis. For each pipe  $i$ , we thus have a relative field density with two components  $d_{i,n}$  and  $d_{i,m}$ . To estimate the total  $\{m, n\}$  of each string, we must therefore sum over the two components separately, weighting with the geometrical overlap of the pipes, such that:

$$m = \sum_{i=0}^N C_i d_{i,m} \quad \text{and} \quad n = \sum_{i=0}^N C_i d_{i,n}, \quad (\text{C.8})$$

where  $C_i$  is the geometrical overlap with pipe  $i$ , there are  $N$  pipes in an event. (Note that the geometrical overlap of an object with itself will always be 1.) These numbers are rounded off to integers  $m$  and  $n$  corresponding to the number of interfering colour charges and anticharges in the rope. To find the relevant colour multiplet  $\{p, q\}$  for the rope, we add  $m$  triplets and  $n$  antitriplets (parallel and anti-parallel strings) with random colours, as described in section 3.1 and appendix B.1. The  $n + m$  strings in the rope should then fragment in a sequential way in  $p + q$  steps, with a gradually decreasing effective tension. This is technically difficult to implement using the PYTHIA implementation of the Lund fragmentation model. In this first study we therefore make an approximation, where we use the average value for  $\tilde{\kappa}$ , given by  $\kappa_{rope}/(p + q)$  with  $\kappa_{rope}$  determined by eq. (3.3). Thus the enhancement factor  $h$  becomes:

$$h = \frac{\langle \tilde{\kappa} \rangle}{\kappa} = \frac{p^2 + pq + q^2 + 3p + 3q}{4(p + q)}. \quad (\text{C.9})$$

The averaging described here will not properly take into account the situation where two triplets become an anti-triplet instead of a sextet. (Note that the situation where a triplet and an antitriplet form a singlet is taken care of by the swing described in section 4.1.) To account for this, we throw away strings in a multiplet with probability  $1 - \frac{p+q}{m+n}$ . A string that is discarded in this way, is simply not hadronized, and will not appear in the final state. Removing strings in this way will have an effect on total multiplicity, which can largely be tuned away, but more seriously, it will break energy–momentum conservation. We have therefore devised a more elaborate scheme in the dipole-based treatment, which will be presented next.

## C.2 A dipole-based treatment

After the final-state shower in ARIADNE, the string can be seen as a chain of dipoles connected by gluons, and in the string fragmentation in PYTHIA8 the break-ups of the string basically follow these dipoles in momentum space. The dipoles, together with their respective overlaps, are thus the basic structures considered in the more sophisticated dipole-based treatment. We study one dipole at a time in its own rest frame, with its two partons along the  $z$ -axis. All other dipoles in the event are boosted to the same frame before calculating their overlap with the dipole under study, using the rapidity span and transverse distance of each of them. As gluons are massless, the rapidity span of a dipole can in principle become infinite, and we therefore use a small gluon mass,  $m_0 \propto 1/r_0 \sim 0.2$  GeV, to limit the rapidities. To allow for a finite formation time of the string pieces between the partons in a dipole, we let the partons propagate in space a fixed time before calculating the transverse distances.<sup>13</sup> For a pair of dipoles, we can now make a linear interpolation between the transverse positions of their respective partons, and we can thus calculate their overlap as the region in rapidity where the two string pieces are closer than  $r_0$ .

Just as in the pipe-based procedure, the colour charges in the dipoles are assumed to be random, although they have a definite direction. We therefore calculate separately the summed overlap of parallel and antiparallel dipoles as

$$m_i = \sum_{j_+ \neq i} \frac{\delta y_{i(j_+)}}{\Delta y_i} \quad \text{and} \quad n_i = \sum_{j_- \neq i} \frac{\delta y_{i(j_-)}}{\Delta y_i}. \quad (\text{C.10})$$

With these overlaps (rounded to integers) we now perform a random walk in colour space to arrive at a multiplet  $(p_i, q_i)$  for the dipole. The random walk is, however, somewhat restricted due to the final-state swing mechanism. If, *e.g.*, we find that  $m = 0$  and  $n = 1$  and add a triplet, we only allow the step  $\{1, 0\} \rightarrow \{1, 1\}$  in colour space, since the swing is assumed to have taken care of the step  $\{1, 0\} \rightarrow \{0, 0\}$  already.

If we had a proper procedure for the junction swing in figure 6 we could have limited the random walk further, *e.g.* with  $m = 1$  and  $n = 0$  we would only allow  $\{1, 0\} \rightarrow \{2, 0\}$  and not  $\{1, 0\} \rightarrow \{0, 1\}$ , and we would always end up in the highest possible multiplet  $\{m, n\}$ . However, since the current version of PYTHIA8 only can handle a limited number of junctions, we have to allow such steps and will end up with dipoles with  $p_i < m$  or  $q_i < n$ , which then corresponds to a partial attenuation of the colour field of the dipole by other nearby dipoles.

If we consider two completely overlapping dipoles which are in the multiplet  $\{0, 1\}$  this would correspond to the right hand side of figure 6, where we basically only have one string piece to be hadronized. To avoid junctions, we therefore break one of the dipoles by replacing the two gluons with a diquark and antiquark. In this way we should get approximately the right multiplicity from the string piece that is left (although its colour flow is reversed compared to a proper junction treatment) and also get the same number of (anti-)baryons that would otherwise have come from the junctions. However, it should

---

<sup>13</sup>The propagation time should be of the order of  $r_0$ , and the effect of this propagation turns out to be very similar to simply reducing the transverse thickness of the string pieces.

be noted that two connected junctions will not necessarily result in a baryon–anti-baryon pair. As we have seen in section 2.4, the popcorn model for baryon production assumes that  $q\bar{q}$  fluctuations that do not break the string occur fairly frequently, allowing additional fluctuations to tunnel out as diquark–antidiquark pairs by locally reversing the colour flow. In the case of a string piece connecting two nearby junctions, these fluctuations may actually again turn the colour flow around, and the  $\bar{q}$  ( $q$ ) from the fluctuation may very well travel along the string and combine with one of the (anti-)quarks in the nearby junction. Note that the probability for this to happen is higher than the probability for the corresponding diquark–antidiquark breakup of a string, since it does not involve the tunneling probability for the heavier diquarks in eq. (2.2). Thus the probability of having a fluctuation, which prevents a baryon–antibaryon pair to result from two connected junctions, should only be governed by the  $\beta$ -parameter in eq. (C.5). Therefore, we will not always break the dipole by introducing diquarks, but with a probability  $\beta$  we will instead use quarks.

This procedure is generalized, so that if a given dipole has overlaps  $m_i$  and  $n_i$  resulting in a multiplet  $(p_i, q_i)$ , the dipole is broken up with a probability  $(1 + m_i + n_i - p_i - q_i)/(1 + m_i + n_i)$ . We note that it may happen that a dipole cannot break up, *e.g.* if the dipole ends are quarks rather than gluons. In this case the probability is modified to increase the probability for the other overlapping dipoles to break by replacing the denominator by  $(1 + m'_i + n'_i)$  where  $m'_i$  and  $n'_i$  are calculated as in eq. (C.10), but only summing over breakable dipoles.

For the dipoles that are left, we can now start the hadronization. To further increase the amount of fluctuations included, we do not average over all breakups, but hadronize each string piece with a local effective string tension

$$\tilde{\kappa} = \tilde{\kappa}(p, q) - \tilde{\kappa}(p - 1, q) = \frac{1}{4} (2 + 2p + q). \quad (\text{C.11})$$

Note that while the expression in eq. (3.3) is symmetric in  $p$  and  $q$ , eq. (C.11) is not. Hadronizing one string at a time implies a choice of whether *this* string is in the  $p$  or  $q$  direction, and here the implicit choice is taken towards the  $p$  direction. The choice is of course still arbitrary, with no effect on the result. The strings are then sent to be hadronized one at a time by PYTHIA8, utilizing a customization described in appendix C.3. This customization enables PYTHIA8 to change hadronization parameters for each string breakup, according to the calculated value of the effective string tension.

### C.3 Implementation details

The implementation of the rope production, through estimation of  $m$  and  $n$  by either an approach based on enclosing cylinders or an approach based on dipoles, followed by a random walk procedure is extensively described in section 4.2, and shall not be repeated. The use of PYTHIA for hadronization, and consequently changing hadronization parameters in a PYTHIA run, is however not part of standard usage of the program, and will be described briefly here. The basic idea is to use PYTHIA to hadronize one string at a time, with the ability to change hadronization parameters while the string is being hadronized, based on the local string tension at that particular point on the string. Since PYTHIA normally



sets hadronization parameters once and for all, when the program is initialized, a feature to intercept the hadronization loop was introduced. In PYTHIA such interceptions are done with so-called `UserHooks`, which in turn allows for re-initialization of parameters. The DIPSY program then delivers a single string to PYTHIA, which calls back for new hadronization parameters every time a step is made. Owing to the interpretation of strings as dipoles connected with gluons introduced in section C.2, the callback needs to include information about which dipole PYTHIA has reached, as well as the position in the dipole. This is done by comparing the invariant mass of all hadrons made from each string end so far, to the invariant mass of the dipoles, starting from the same string end. This relies on PYTHIA and DIPSY having identical, fixed string ends when the hadronization procedure begins. This is not the case for gluon loops, as PYTHIA will first cut one dipole at random, with probability proportional to invariant mass squared. As an approximation, gluon loops are hadronized with the average value of the string tension for the whole string. Thus, parameters need to be set only once for gluon loops.

## D. Tuning

To ensure that the observables of main interest for rope formation, such as the rates of baryons and strange hadrons, are not affected by global flavour independent effects on particle spectra, we made a complete tuning of relevant parameters in DIPSY, ARIADNE and PYTHIA8, with and without inclusion of our new rope models. For this we have used a selection of data analyses from the Rivet program [91], and used the Professor framework [92] for the actual tuning.

### D.1 Tuning final-state shower and hadronization

We followed the standard procedure of first tuning the parameters in the final-state shower (in ARIADNE) and in the hadronization (in PYTHIA8) to  $e^+e^-$ -observables as measured at LEP. It can be noted that the old Fortran version of ARIADNE has already been tuned to such data with very good results (see *e.g.* ref. [93]), and since the final-state shower in ARIADNE is basically unchanged in the new version, we obtain equally good results for the default version. When we now add the final-state swing and rope fragmentation we do not expect the results to change very much, as the number of dipoles produced are fairly low, and do not allow for many reconnections. We do expect some changes in parameters, however, since the swing tends to decrease the total string lengths and therefore also the multiplicity. Indeed, we find that *e.g.* the tuned value for the  $a$  parameter in the fragmentation is somewhat increased when the swing is included.

In figure 18 we show two distributions used in the tuning. We find that the thrust distribution is equally well described with and without swing. This is expected since it should be dominated by effects from the hardest gluon emission, and by construction there are no effects of the swing for the first two emissions. For the transverse momentum distribution out of the event plane (defined by the thrust major and minor axes) we do, however, find some differences. Here we should be dominated by the two hardest gluon emissions, and there we can expect larger effects from the swing in subsequent emissions

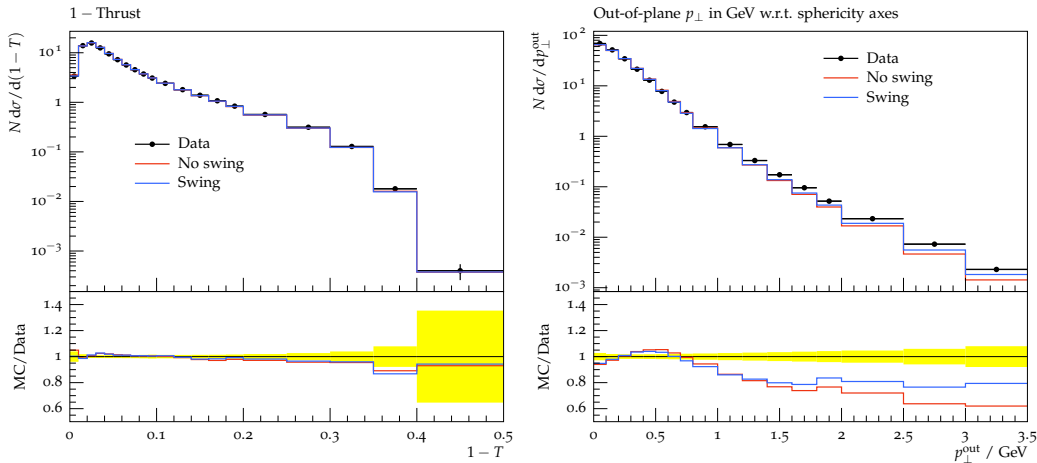


**Figure 18:** Sample plots from tuning of the ARIADNE dipole shower with string fragmentation from PYTHIA8 to DELPHI data [93], with and without final state swing. On the left is shown the distribution in thrust, and on the right the distribution of transverse momenta out of the event plane.

and in the hadronization. We see that the description of data is somewhat improved, and in general the total  $\chi^2/Ndf.$  is also somewhat improved when the swing is included.

Note that we do not expect any effects of the rope hadronization in  $e^+e^- \rightarrow \text{hadrons}$ , as we should be dominated by a single string. In high multiplicity events there could be some internal overlaps but we found<sup>14</sup> no change in the tuned observables when including the ropes.

## D.2 Tuning DIPSY

We then proceed to tune the parameters of the DIPSY model to  $pp$  collisions. Here we tune both to the total and elastic cross sections as well as to final-state observables in minimum bias events. It should be emphasized that the DIPSY program is not yet ready for precision description of final-state observables. Although the model has improvements beyond the leading logarithmic BFKL accuracy, there are no proper matrix elements included for hard scatterings and there are no quarks included in the evolution. We therefore do not expect it to be able to give a good description of observables involving high transverse momenta, and indeed we find that the particle rates above  $p_\perp \sim 5$  GeV are severely overestimated. In addition we have found that, although the energy dependence of the total, elastic, and diffractive cross sections are well reproduced, the energy dependence of the total multiplicity is a bit too flat. We therefore decided to make separate tunes for different collision energies as well as global tunes. As it turned out that the observables in section 5, were insensitive to whether we used separate or global tunes, we there only present results using the latter.

<sup>14</sup>In  $e^+e^- \rightarrow \text{hadrons}$  we use the thrust axis rather than the beam axis to define the rapidity span of strings for the pipe-based treatment.

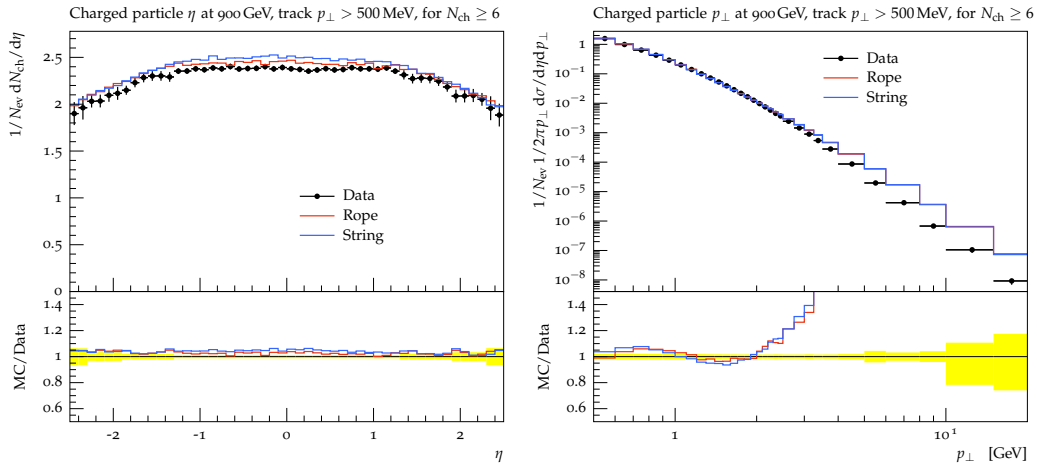


**Figure 19:** Sample plots from the tuning of DIPSY to 900 GeV  $pp$  minimum-bias data from ATLAS [94]. On the left is shown the pseudo-rapidity distribution of charged particles with transverse momenta larger than 500 MeV in events with at least six charged particles. On the right is given the transverse momentum distribution of charged particles for the same events. In both plots the lines labelled *Rope* is DIPSY with the new (dipole-based) rope model, while *String* indicates DIPSY with the standard fragmentation. In both cases the final-state swing model is used.

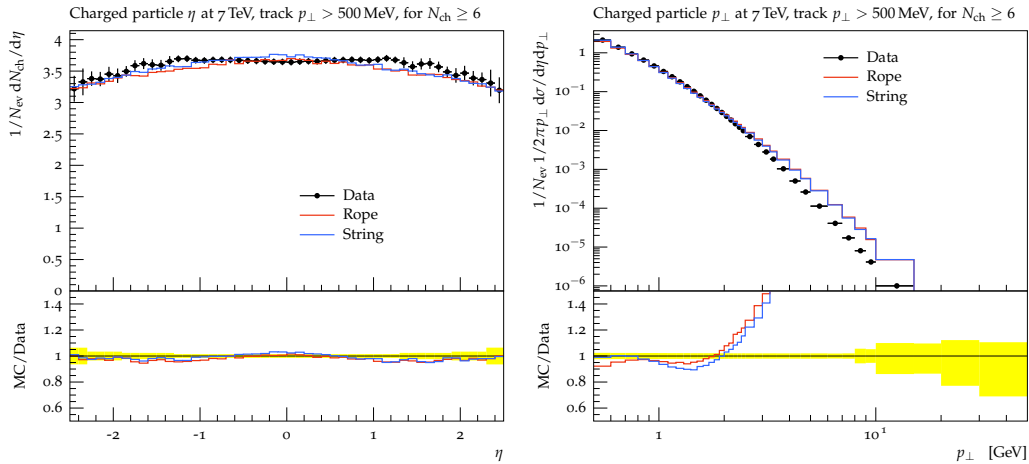


**Figure 20:** Sample plots from the tuning of DIPSY to 7 TeV  $pp$  minimum-bias data from ATLAS [94], using the same distributions and models as in figure 19.

In figures 19 and 20 we show examples of observables used in the tuning of 900 GeV and 7 TeV respectively. The rapidity distribution of charged particles is well described for both energies and both for the default fragmentation and for the rope model. While above a couple of GeV, the transverse momentum distribution in all cases is too hard, the average transverse momenta are well described as shown in figure 21. In a future publication we intend to try to cure these deficiencies, but here we are satisfied that we obtain very similar results with and without ropes.

Since DIPSY in the current version does not describe diffractive final states (see [16]), it is necessary to choose observables for comparison which are not greatly affected by

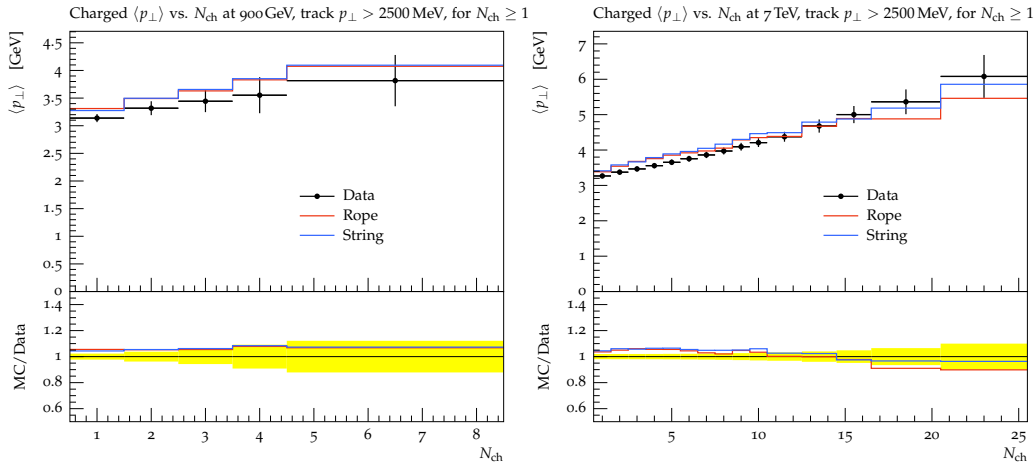


**Figure 21:** Sample plots from the tuning of DIPSY to 900 GeV (left) and 7 TeV (right)  $pp$  minimum-bias data from ATLAS [94]. Both plots show the average transverse momenta (above 2.5 GeV) as a function of the number of charged particles per event. The models are the same as in figure 19.

the presence of diffractive events. This is important both for the tuning and for the observables studied in section 5.1. In PYTHIA8 it is possible to turn on and off the diffractive contributions, and such runs can be used to determine which observables should be used for the present analysis. As an example we show in figure 22 a comparison between results from PYTHIA8 and data from CMS for the rapidity distribution of  $\Lambda$  (figure 22 (left)) and the ratio  $K_s^0/\Lambda$  in figure 22 (right). It is clear that the inclusion of diffractive events plays a great role when looking at raw per-event distributions. In PYTHIA8 the diffractive events are hadronizing in the same way as the non-diffractive, and the  $K_s^0/\Lambda$  ratio is therefore not modified by including diffractive events. Even if this is not confirmed by experiments at present, we note that the contribution from diffractive events is relatively small. A moderate difference in particle ratios in diffractive events should therefore not change predictions for particle ratios in a serious way, and such ratios should therefore be better observables in comparisons between our model and data.

Looking at figure 22 it is also directly visible that PYTHIA8 has difficulties reproducing these distributions, which is also the case for almost all contemporary generators (see. *e.g.* `mcplots.cern.ch`)

## References

- [1] T. Sjöstrand, S. Mrenna, and P. Skands, *JHEP* **05** (2006) 026, [arXiv:hep-ph/0603175](#).
- [2] M. Bähr *et al.*, *Eur. Phys. J.* **C58** (2008) 639–707, [arXiv:0803.0883 \[hep-ph\]](#).
- [3] T. S. Biro, H. B. Nielsen, and J. Knoll, *Nuclear Physics B* **245** (1984) 449–468.
- [4] A. Białas and W. Czyz, *Phys.Rev.* **D31** (1985) 198.
- [5] A. K. Kerman, T. Matsui, and B. Svetitsky, *Phys.Rev.Lett.* **56** (1986) 219.
- [6] M. Gyulassy and A. Iwazaki, *Phys.Lett.* **B165** (1985) 157–161.

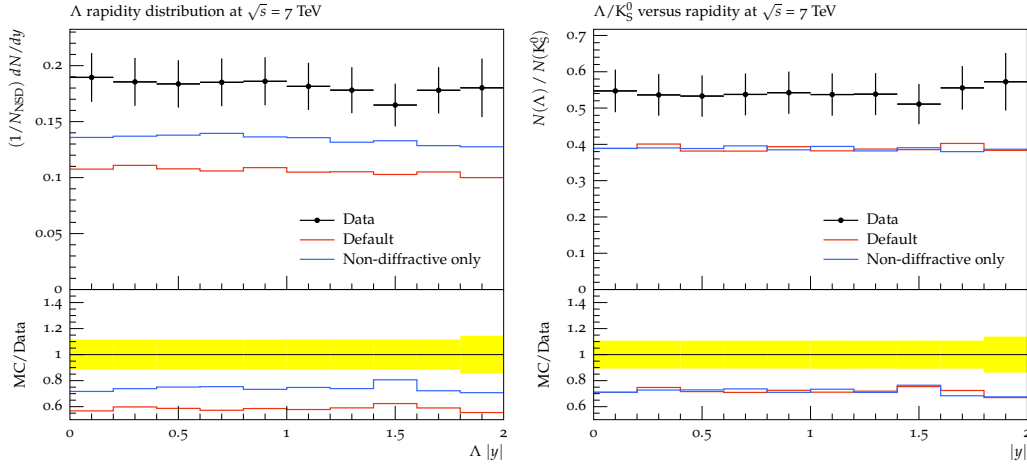


**Figure 22:** Pythia non-diffractive only (blue) and including diffractive (red), compared to 7000 GeV data from CMS for the  $\Lambda$  rapidity distribution (left) and the  $\Lambda/K_s^0$  ratio (right).

- [7] B. Andersson and P. Henning, *Nucl.Phys.* **B355** (1991) 82–105.
- [8] M. Braun and C. Pajares, *Nucl.Phys.* **B390** (1993) 542–558.
- [9] M. Braun and C. Pajares, *Phys.Rev.* **D47** (1993) 114–122.
- [10] N. Amelin, M. Braun, and C. Pajares, *Z.Phys.* **C63** (1994) 507–516.
- [11] N. Armesto, M. Braun, E. Ferreiro, and C. Pajares, *Phys.Lett.* **B344** (1995) 301–307.
- [12] K. Kajantie and T. Matsui, *Phys.Lett.* **B164** (1985) 373.
- [13] G. Gatoff, A. Kerman, and T. Matsui, *Phys.Rev.* **D36** (1987) 114.
- [14] M. Braun, C. Pajares, and J. Ranft, *Int.J.Mod.Phys.* **A14** (1999) 2689–2704, [arXiv:hep-ph/9707363](#) [hep-ph].
- [15] E. Avsar, G. Gustafson, and L. Lönnblad, *JHEP* **07** (2005) 062, [hep-ph/0503181](#).
- [16] C. Flensburg, G. Gustafson, and L. Lönnblad, *JHEP* **1108** (2011) 103, [arXiv:1103.4321](#) [hep-ph].
- [17] C. Merino, C. Pajares, and J. Ranft, *Phys.Lett.* **B276** (1992) 168–172.
- [18] H. Möhring, J. Ranft, C. Merino, and C. Pajares, *Phys.Rev.* **D47** (1993) 4142–4145.
- [19] H. Sorge, M. Berenguer, H. Stoecker, and W. Greiner, *Phys.Lett.* **B289** (1992) 6–11.
- [20] M. Bleicher, W. Greiner, H. Stoecker, and N. Xu, *Phys.Rev.* **C62** (2000) 061901, [arXiv:hep-ph/0007215](#) [hep-ph].
- [21] S. Soff, J. Randrup, H. Stoecker, and N. Xu, *Phys.Lett.* **B551** (2003) 115–120, [arXiv:nucl-th/0209093](#) [nucl-th].
- [22] B. Andersson, G. Gustafson, and B. Söderberg, *Z. Phys.* **C20** (1983) 317.
- [23] B. Andersson and G. Gustafson, *Z.Phys.* **C3** (1980) 223.
- [24] B. Andersson, G. Gustafson, G. Ingelman, and T. Sjöstrand, *Phys. Rept.* **97** (1983) 31.

- [25] A. Buckley, J. Butterworth, S. Gieseke, D. Grellscheid, S. Höche, *et al.*, [arXiv:1101.2599](#) [[hep-ph](#)].
- [26] K. Hamacher and M. Weierstall, [hep-ex/9511011](#).
- [27] T. Sjöstrand, S. Ask, J. R. Christiansen, R. Corke, N. Desai, *et al.*, [arXiv:1410.3012](#) [[hep-ph](#)].
- [28] A. Casher, H. Neuberger, and S. Nussinov, *Phys.Rev.* **D20** (1979) 179–188.
- [29] B. Andersson, G. Gustafson, and T. Sjöstrand, *Z.Phys.* **C6** (1980) 235.
- [30] E. Gurvich, *Phys.Lett.* **B87** (1979) 386–388.
- [31] N. Glendenning and T. Matsui, *Phys.Rev.* **D28** (1983) 2890–2891.
- [32] J. S. Schwinger, *Phys. Rev.* **82** (1951) 664–679.
- [33] E. Brezin and C. Itzykson, *Phys. Rev.* **D2** (1970) 1191–1199.
- [34] **UA5 Collaboration** Collaboration, G. Alner *et al.*, *Nucl.Phys.* **B258** (1985) 505.
- [35] **H1 Collaboration** Collaboration, F. Aaron *et al.*, *Eur.Phys.J.* **C61** (2009) 185–205, [arXiv:0810.4036](#) [[hep-ex](#)].
- [36] **CMS Collaboration** Collaboration, V. Khachatryan *et al.*, *JHEP* **1105** (2011) 064, [arXiv:1102.4282](#) [[hep-ex](#)].
- [37] J. Ambjørn, P. Olesen, and C. Peterson, *Nucl.Phys.* **B240** (1984) 533.
- [38] G. S. Bali, *Phys.Rev.* **D62** (2000) 114503, [arXiv:hep-lat/0006022](#) [[hep-lat](#)].
- [39] A. H. Mueller, *Nucl. Phys.* **B415** (1994) 373–385.
- [40] A. H. Mueller and B. Patel, *Nucl. Phys.* **B425** (1994) 471–488, [hep-ph/9403256](#).
- [41] A. H. Mueller, *Nucl. Phys.* **B437** (1995) 107–126, [hep-ph/9408245](#).
- [42] L. D. McLerran and R. Venugopalan, *Phys.Rev.* **D49** (1994) 2233–2241, [arXiv:hep-ph/9309289](#) [[hep-ph](#)].
- [43] L. D. McLerran and R. Venugopalan, *Phys.Rev.* **D49** (1994) 3352–3355, [arXiv:hep-ph/9311205](#) [[hep-ph](#)].
- [44] C. Flensburg, G. Gustafson, L. Lönnblad, and A. Ster, *JHEP* **06** (2011) 066, [arXiv:1103.4320](#) [[hep-ph](#)].
- [45] C. Flensburg and G. Gustafson, *JHEP* **1010** (2010) 014, [arXiv:1004.5502](#) [[hep-ph](#)].
- [46] C. Flensburg, G. Gustafson, and L. Lönnblad, *JHEP* **1212** (2012) 115, [arXiv:1210.2407](#) [[hep-ph](#)].
- [47] C. Flensburg, [arXiv:1108.4862](#) [[nucl-th](#)].
- [48] C. Flensburg, *Prog.Theor.Phys.Suppl.* **193** (2012) 172–175.
- [49] K. G. Wilson, *Phys. Rev.* **D10** (1974) 2445–2459.
- [50] B. Andersson and G. Gustafson, “Why are Vector Mesons Suppressed in Jet Fragmentation?.” Lund preprint, LU-TP-82-5 (1982).
- [51] B. Andersson, G. Gustafson, and T. Sjöstrand, *Nucl.Phys.* **B197** (1982) 45.
- [52] B. Andersson, G. Gustafson, and T. Sjöstrand, *Phys.Scripta* **32** (1985) 574.

- [53] S. Jeon and R. Venugopalan, *Phys.Rev.* **D70** (2004) 105012, [arXiv:hep-ph/0406169](#) [[hep-ph](#)].
- [54] K. Johnson, *Acta Phys.Polon.* **B6** (1975) 865.
- [55] K. Johnson and C. B. Thorn, *Phys.Rev.* **D13** (1976) 1934.
- [56] C. Semay, *Eur.Phys.J.* **A22** (2004) 353–354, [arXiv:hep-ph/0409105](#) [[hep-ph](#)].
- [57] M. Cardoso, N. Cardoso, and P. Bicudo, *Phys.Rev.* **D81** (2010) 034504, [arXiv:0912.3181](#) [[hep-lat](#)].
- [58] P. Cea, L. Cosmai, F. Cuteri, and A. Papa, *Phys.Rev.* **D89** (2014) 094505, [arXiv:1404.1172](#) [[hep-lat](#)].
- [59] E. Avsar, G. Gustafson, and L. Lönnblad, *JHEP* **01** (2007) 012, [hep-ph/0610157](#).
- [60] E. Avsar, G. Gustafson, and L. Lönnblad, *JHEP* **12** (2007) 012, [arXiv:0709.1368](#) [[hep-ph](#)].
- [61] E. A. Kuraev, L. N. Lipatov, and V. S. Fadin, *Sov. Phys. JETP* **45** (1977) 199–204.
- [62] I. I. Balitsky and L. N. Lipatov, *Sov. J. Nucl. Phys.* **28** (1978) 822–829.
- [63] G. Gustafson, *Phys. Lett.* **B175** (1986) 453.
- [64] G. Gustafson and U. Pettersson, *Nucl. Phys.* **B306** (1988) 746.
- [65] L. Lönnblad, *Comput. Phys. Commun.* **71** (1992) 15–31.
- [66] T. Sjöstrand, S. Mrenna, and P. Skands, *Comput. Phys. Commun.* **178** (2008) 852–867, [arXiv:0710.3820](#) [[hep-ph](#)].
- [67] L. Lönnblad, *Z.Phys.* **C70** (1996) 107–114.
- [68] T. Sjöstrand and M. van Zijl, *Phys. Rev.* **D36** (1987) 2019.
- [69] G. Gustafson, U. Pettersson, and P. Zerwas, *Phys.Lett.* **B209** (1988) 90.
- [70] T. Sjöstrand and V. A. Khoze, *Phys.Rev.Lett.* **72** (1994) 28–31, [arXiv:hep-ph/9310276](#) [[hep-ph](#)].
- [71] A. Edin, G. Ingelman, and J. Rathsman, *Phys.Lett.* **B366** (1996) 371–378, [arXiv:hep-ph/9508386](#) [[hep-ph](#)].
- [72] R. Enberg, G. Ingelman, and N. Timneanu, *Phys.Rev.* **D64** (2001) 114015, [arXiv:hep-ph/0106246](#) [[hep-ph](#)].
- [73] B. Andersson, G. Gustafson, and B. Söderberg, *Nucl.Phys.* **B264** (1986) 29.
- [74] B. Andersson, P. Dahlkvist, and G. Gustafson, *Phys.Lett.* **B214** (1988) 604–608.
- [75] L. Lönnblad, *Nucl.Instrum.Meth.* **A559** (2006) 246–248.
- [76] A. Karneyeu, L. Mijovic, S. Prestel, and P. Skands, *Eur.Phys.J.* **C74** (2014) 2714, [arXiv:1306.3436](#) [[hep-ph](#)].
- [77] **STAR Collaboration** Collaboration, J. Adams *et al.*, *Phys.Lett.* **B637** (2006) 161–169, [arXiv:nucl-ex/0601033](#) [[nucl-ex](#)].
- [78] K. Werner, B. Guiot, I. Karpenko, and T. Pierog, [arXiv:1411.1048](#) [[nucl-th](#)].
- [79] N. Armesto, N. Borghini, S. Jeon, U. Wiedemann, S. Abreu, *et al.*, *J.Phys.* **G35** (2008) 054001, [arXiv:0711.0974](#) [[hep-ph](#)].

- [80] A. Ortiz Velasquez, P. Christiansen, E. Cuautle Flores, I. Maldonado Cervantes, and G. Paić, *Phys.Rev.Lett.* **111** (2013) 042001, [arXiv:1303.6326 \[hep-ph\]](#).
- [81] **ALICE Collaboration** Collaboration, B. B. Abelev *et al.*, *Phys.Lett.* **B736** (2014) 196–207, [arXiv:1401.1250 \[nucl-ex\]](#).
- [82] R. Engel and J. Ranft, *Phys.Rev.* **D54** (1996) 4244–4262, [arXiv:hep-ph/9509373 \[hep-ph\]](#).
- [83] J. M. Butterworth, J. R. Forshaw, and M. H. Seymour, *Z. Phys.* **C72** (1996) 637–646, [hep-ph/9601371](#).
- [84] V. S. Fadin and L. N. Lipatov, *Phys. Lett.* **B429** (1998) 127–134, [hep-ph/9802290](#).
- [85] M. Ciafaloni and G. Camici, *Phys. Lett.* **B430** (1998) 349–354, [hep-ph/9803389](#).
- [86] G. P. Salam, *Acta Phys. Polon.* **B30** (1999) 3679–3705, [hep-ph/9910492](#).
- [87] J. Kwiecinski, A. D. Martin, and P. J. Sutton, *Z. Phys.* **C71** (1996) 585–594, [hep-ph/9602320](#).
- [88] B. Andersson, G. Gustafson, and J. Samuelsson, *Nucl. Phys.* **B467** (1996) 443–478.
- [89] I. Balitsky, *Nucl. Phys.* **B463** (1996) 99–160, [hep-ph/9509348](#).
- [90] Y. V. Kovchegov, *Phys. Rev.* **D60** (1999) 034008, [hep-ph/9901281](#).
- [91] A. Buckley *et al.*, [arXiv:1003.0694 \[hep-ph\]](#).
- [92] A. Buckley, H. Hoeth, H. Lacker, H. Schulz, and J. E. von Seggern, *Eur.Phys.J.* **C65** (2010) 331–357, [arXiv:0907.2973 \[hep-ph\]](#).
- [93] **DELPHI Collaboration**, P. Abreu *et al.*, *Z. Phys.* **C73** (1996) 11–60.
- [94] **ATLAS Collaboration** Collaboration, G. Aad *et al.*, *New J.Phys.* **13** (2011) 053033, [arXiv:1012.5104 \[hep-ex\]](#).